

Variation in chemical composition and sources of PM_{2.5} during the COVID-19 lockdown in Delhi

Chirag Manchanda ^a, Mayank Kumar ^{a,*}, Vikram Singh ^{b,*}, Mohd Faisal ^b, Naba Hazarika ^c, Ashutosh Shukla ^d, Vipul Lalchandani ^d, Vikas Goel ^a, Navaneeth Thamban ^d, Dilip Ganguly ^e, Sachchida Nand Tripathi ^{d,*}

a. Department of Mechanical Engineering, Indian Institute of Technology, Delhi, New Delhi, India

b. Department of Chemical Engineering, Indian Institute of Technology, Delhi, New Delhi, India

c. Department of Applied Mechanics, Indian Institute of Technology, Delhi, New Delhi, India

d. Department of Civil Engineering, Indian Institute of Technology, Kanpur, Uttar Pradesh, India

e. Centre for Atmospheric Sciences, Indian Institute of Technology, Delhi, New Delhi, India

Abstract

The Government of India (GOI) announced a nationwide lockdown starting 25th March 2020 to contain the spread of COVID-19, leading to an unprecedented decline in anthropogenic activities and in turn improvements in ambient air quality. This is the first study to focus on highly time-resolved chemical speciation and source apportionment of PM_{2.5} to assess the impact of the lockdown and subsequent relaxations on the sources of ambient PM_{2.5} in Delhi, India. The elemental, organic, and black carbon fractions of PM_{2.5} were measured at the IIT Delhi campus from February 2020 to May 2020. We report source apportionment results using positive matrix factorization (PMF) of organic and elemental fractions of PM_{2.5} during the different phases of the lockdown. The resolved sources such as vehicular emissions, domestic coal combustion, and semi-volatile oxygenated organic aerosol (SVOOA) were found to decrease by 96%, 95%, and 86%, respectively, during lockdown phase-1 as compared to pre-lockdown. An unforeseen rise in O₃ concentrations with declining NO_x levels was observed, similar to other parts of the globe, leading to the low-volatility oxygenated organic aerosols (LVOOA) increasing to almost double the pre-lockdown concentrations during the last phase of the lockdown. The effect of the lockdown was found to be less pronounced on other resolved sources like secondary chloride, power plants, dust-related, hydrocarbon-like organic aerosols (HOA), and biomass burning related emissions, which were also swayed by the changing meteorological conditions during the four lockdown phases. The results presented in this study provide a basis for future emission control strategies, quantifying the extent to which

* Corresponding Authors

E-mail addresses : kmayank@mech.iitd.ac.in (M. Kumar); vs225@chemical@iitd.ac.in (V. Singh); snt@iitk.ac.in (S.N. Tripathi)

constraining certain anthropogenic activities can ameliorate the ambient air. These results have direct relevance to not only Delhi but the entire Indo-Gangetic plain (IGP) citing similar geographical and meteorological conditions common to the region along with overlapping regional emission sources.

Summary of main findings

We identify sources like vehicular emissions, domestic coal combustion, and semi-volatile oxygenated organic aerosol (SVOOA) to be severely impacted by the lockdown whereas ozone levels and in turn low-volatility oxygenated organic aerosols (LVOOA) rise by more than 95% compared to the pre-lockdown concentrations during the last phase of the lockdown. However, other sources resolved in this study like secondary chloride, power plants, dust-related, hydrocarbon-like organic aerosols (HOA), and biomass burning related emissions, were mainly driven by the changes in the meteorological conditions rather than the lockdown.

Keywords:

COVID-19 Lockdown; Source Apportionment; PM_{2.5}; Delhi; Air Pollution; Elemental and organic fractions

Introduction

The progression of air pollutants from its source to the receptor is often governed by a multitude of transport processes (advective winds, convective updraft or turbulent diffusion) and multiphase transformations. These transformations are often effected by chemical reactions that lead to heterogeneous mass transfer, which further complicates the system. Thus the concentration of each pollutant is often dependent on the concentration of other pollutants through a series of chemical reactions (Seinfeld, 2004). Time-resolved measurements of concentration and chemical composition of these aerosols provide valuable insights into the levels of air pollution (Fehsenfeld, 2004). However, measurements alone are limited in space and time and are unable to provide much information on the origin or source of these pollutants. This has led to the widespread use of various data analysis/source apportionment techniques in the last few decades, to extract more information on the nature and composition of emission sources (Watson and Chow, 2015). However, secondary pollutants display a highly non-linear relationship with precursor emissions; thus, source apportionment techniques are unable to provide any information to predict the effect of increase/decrease of precursor emissions on secondary pollutant concentrations (Burr and Zhang, 2011).

The COVID-19 induced lockdown around different parts of the globe resulted in an unprecedented impact on the environment, with a drastic reduction in primary emissions; thus, enabling us to evaluate the impact of reduced precursor concentrations on secondary aerosols, allowing us to better understand the dominant formation mechanism for a

particular secondary pollutant in a given setting. The first lockdown was enforced in various parts of the Hubei province in China from 23rd January 2020, followed by similar measures in other cities (Wu et al., 2020). The COVID-19 outbreak was declared to be a pandemic by the World Health Organization (WHO) on 11th March 2020 (Sohrabi et al., 2020), following which lockdown or similar restricted movement measures were implemented in different parts of the world.

An early study by Bao and Zhang (2020) analyzed the impact of reduced human mobility due to the lockdown, on ambient air quality in 44 cities in Northern China from January to March 2020. The study found the average AQI to decrease by 7.8%, while significant pollutants like SO₂, PM_{2.5}, PM₁₀, NO₂, and CO, decreased 6.76%, 5.93%, 13.66%, 24.67%, and 4.58% respectively. A consequent study by Li et al. (2020) utilized the Particulate Source Apportionment Technology (PSAT) coupled with the Comprehensive Air quality Model with extensions (CAMx) to quantify contributions from 8 different sources to total PM_{2.5} variations over the Yangtze River Delta (YRD) region, with the study period spanning 1st January to 31st March 2020 and the most stringent lockdown lasting from 24th January to 25th February 2020. Significant reductions in industrial operations, vehicular kilometers traveled (VKT), construction, and other anthropogenic activities were observed, in turn, bringing about a 25.4% to 48.1% decrease in PM_{2.5} concentrations at different sites over the YRD region. However, an average rebound of 20.5% was recorded for ozone concentration. This anomaly was attributed to the fact that a significant drop in the NO_x concentration was observed (29.5% to 51.7%). At the same time, the reduction in VOC was not as intense as NO_x leading to a drop in titration effect towards ozone (Seinfeld, J.H. and Pandis, 2006).

Such increase in regional oxidation capacity effected by the rise in ozone concentration due to decrease in NO_x in a VOC-limited environment during the lockdown was also reported in several other independent studies; Lv et al. (2020) for Beijing (China); Zheng et al. (2020) for Wuhan (China); Sicard et al. (2020) for Wuhan (China), Nice (France), Rome (Italy), Turin (Italy), Valencia (Spain); Tobías et al. (2020) for Barcelona (Spain); Mahato et al. (2020) for Delhi (India), Selvam et al. (2020) for Gujrat (India), Kumari and Toshniwal (2020) for Delhi (India) and Mumbai (India).

In India, the nationwide lockdown was implemented on 24th March 2020 and lasted up till 31st May 2020, with phase-wise relaxations starting 19th April 2020. Mahato et al. (2020) published an early work quantifying the impact of the first phase of the lockdown on ambient air quality in the Delhi-NCT region. The study reported average PM_{2.5} and PM₁₀ concentrations to dip by 53% and 52% respectively when compared to the pre-lockdown, while SO₂, NO₂, CO, and NH₃ were found to decrease by 18%, 53%, 30%, and 12% respectively. Similar trends in PM_{2.5}, SO₂, NO₂, and CO concentrations were observed independently by Srivastava et al. (2020) in both Lucknow and Delhi, by Kumari and Toshniwal (2020) in Delhi, Mumbai, and Singrauli and by Selvam et al. (2020) in Gujrat. However, the reduction in

SO₂ was found to be more pronounced in Mumbai (39%) Gujarat (48%), and was attributed to their closeness to the ocean and, thus, shipping emissions, by Selvam et al. (2020) and Kumari and Toshniwal (2020).

Despite these early studies investigating the impact of the lockdown in India, there has been no study focusing on the variation of the sources and chemical composition of particulate matter during different phases of the lockdown or the impact of increased O₃ concentrations on the sources of PM_{2.5}. The present study is aimed at studying the highly time-resolved variation of sources contributing to both the organic and inorganic fragments of PM_{2.5}, from pre-lockdown through each phase of the lockdown. These results aid us in quantifying the impact that reduction of certain primary emissions can have on overall air quality and the inadvertent effect these reductions can have on secondary aerosols.

2. Experimental Methods and Data Analysis

2.1 Sampling Site and Instrumentation

The sampling was conducted at the campus of Indian Institute of Technology (IIT), Delhi (28°32'N; 77°11'E). The instruments are housed in a temperature-controlled laboratory on the top floor of a four-story building on campus. The nearest source of local emissions is an arterial road outside campus, located about 150m from the building.

The nationwide lockdown was implemented in India for an initial period of 21 days, starting 25th March 2020 until 14th April 2020. The lockdown was extended for another 21 days until 3rd May 2020, with the first set of relaxations to certain agricultural and industrial activities, beginning 20th April 2020. Following the end of lockdown phase-2, the lockdown was further extended twice for a period of 14 days each, with increased allowances focused on restarting of commercial activities, before concluding on 31st May 2020. Further details about the allowances in each phase of the lockdown have been discussed in supplementary information (SI) section 3.

The study period has been subdivided into five phases, such that each subsequent phase coincides with increasing relaxations in the lockdown: Pre-Lockdown (PLD) (24th February – 24th March 2020), effective Lockdown Phase-1 (eLD-1) (25th March -19th April 2020), effective Lockdown Phase-2 (eLD-2) (20th April – 3rd May 2020), Lockdown Phase-3 (LD-3) (4th May – 17th May 2020), Lockdown Phase-4 (LD-4) (18th May – 31st May 2020).

The Xact 625i Ambient Metals Monitor (Cooper Environmental Services, Tigard, Oregon, USA) equipped with a PM_{2.5} inlet was deployed for sampling and was set up to quantify 36 elements with an hourly time resolution. Meanwhile, an Aerosol Chemical Speciation Monitor (ACSM, Aerodyne Inc., MA, USA) was deployed for analyzing the non-refractory particulate matter with an aerodynamic diameter smaller than 2.5µm (NR-PM_{2.5}). The ACSM measured the concentration of organic aerosols along with sulfate, nitrate, ammonium (SNA), and chloride

concentration, with a time resolution of ten minutes. Black Carbon (BC) concentrations were measured using a multichannel Aethalometer (Magee Scientific Model AE33, Berkeley, CA) with a 1-minute time resolution.

Total PM_{2.5} was measured for intermittent periods during the study for data quality assurance or quality control (QA/QC) purposes (Figure S1), using a collocated Beta Attenuation Monitor (BAM 1022, MetOne Instruments Inc., OR, USA), with a 15-min time resolution. Wind Speed (WS) and Wind Direction (WD) were calculated for the nearest grid point to the sampling site, using the Global Forecast System (GFS, NCEP, USA). Relative Humidity (RH), Ambient Temperature (AT), and rainfall were recorded using an onsite Ambient Weather Monitoring station. Ozone, SO₂, CO, and NO_x measurements were taken from the Continuous Ambient Air Quality Monitoring Station (CAAQMS) at RK Puram located at a distance of around 3 km from our sampling site. All CAAQMS stations in Delhi, including the RK Puram station, are managed by either the Central Pollution Control Board (CPCB) or the Delhi Pollution Control Council (DPCC) and together provide a network of near-real time monitoring of PM_{2.5}/PM₁₀ levels, along with major gaseous pollutants. Further details on the instrumentation and QA/QC checks for each instrument are provided in SI section S1.

2.2 Source Apportionment using PMF

This study utilizes Positive Matrix Factorization (PMF) to apportion the measured particulate concentrations to realizable sources. PMF is a standard multivariate factor analysis tool widely used for source apportionment of aerosols (Sharma et al., 2016; Ulbrich et al., 2009; Vossler et al., 2016). The algorithm attempts to best describe the variability in a multivariate input dataset as the linear combination of a set of constant factor profiles and their relative contribution at every corresponding time step, as shown in Eq. (1):

$$x_{ij} = \sum_{k=1}^p g_{ik} f_{kj} + e_{ij} \dots\dots (1)$$

Where x_{ij} is the measured elemental concentration, f_{kj} is the factor/source profile, g_{ik} the time-varying contribution of each source, and e_{ij} represent the elements of the residuals matrix. The indices i and j denote each of the n time steps and m chemical species, while k refers to each factor/source out of total p source profiles, which is defined by the user.

In PMF, each element of the factor matrix is constrained that no sample can have a negative factor contribution. The solution to Eqn. 1 is achieved iteratively by minimizing the object function or the goodness of fit parameter known as Q value:

$$Q = \sum_i \sum_j \left(\frac{e_{ij}}{s_{ij}} \right)^2 \dots\dots (2)$$

Here, s_{ij} corresponds to the measurement uncertainty for every cell of the input matrix x_{ij} . The PMF algorithm was solved using the Multilinear Engine (ME) -2 (Paatero, 1999). In this study, the PMF algorithm was implemented using EPA PMF 5.0 that is built on the ME-2 solution model. A detailed description of the model is provided in past studies (Paatero, 1997; Paatero and Tapper, 1994). Further details on PMF input preparation, factor selection, and uncertainty quantification have been reported in SI section S2.

3. Results and Discussion

The PLD phase in the present study marks the phase with no restricted movement, while eLD-1 corresponds to the phase with the most stringent lockdown. Consequently, the span of each phase from eLD-2 to LD-4 has been concomitant with increments in relaxations to the lockdown (resulting in increased commercial activity and human mobility) as implemented by the state/central government.

Variation in measured $PM_{2.5}$ and its constituents, along with the major gaseous pollutants, are presented in Figure 1 (a-d). We note that the average $PM_{2.5}$ values fall by 53.6% from PLD to eLD-1; this is in line with the findings of Kumari and Toshniwal (2020) and Mahato et al. (2020). The PM levels trend back towards the initial concentrations with increasing relaxations in consequent phases of the lockdown, however, even during LD-4 average $PM_{2.5}$ remained 33% lower compared to the PLD values. A significant drop in NO_2 , NO and CO concentrations 56%, 90%, and 32% (Figure S6(a)) respectively, was recorded during eLD-1, while SO_2 remains largely unaffected by the lockdown. Further discussion on time variations of these gaseous pollutants is presented in SI section 3.1.2.

The effect of the lockdown on secondary aerosol formation is further analyzed using the Sulfate Oxidation Ratio (SOR) and Nitrate Oxidation Ratio (NOR) (Figure 1(d)). The SOR and NOR are defined as the molar ratio of SO_4 and NO_3 to total oxidized S ($SO_4 + SO_2$), and total oxidized N ($NO_3 + NO_x$), respectively (Zhang et al., 2011). The average SOR for the PLD was 0.26, followed by 0.1, 0.15, 0.13, and 0.1 for each of eLD-1 to LD-4, while the average NOR for the PLD was 0.12, followed by 0.07, 0.1, 0.1 and 0.06 for each of eLD-1 to LD-4. According to previous studies, SOR and NOR lower than 0.25 and 0.10, respectively, are a marker for primary particulate matter (Ohta and Okita, 1990). Thus, the reduction in these ratios seems to indicate some role of lockdown in hindering the formation of secondary particles. However, contrary to the nature of total $PM_{2.5}$ and gaseous pollutants, these ratios do not tend towards the PLD values; with increasing relaxations, these ratios achieve the lowest average values in LD-4.

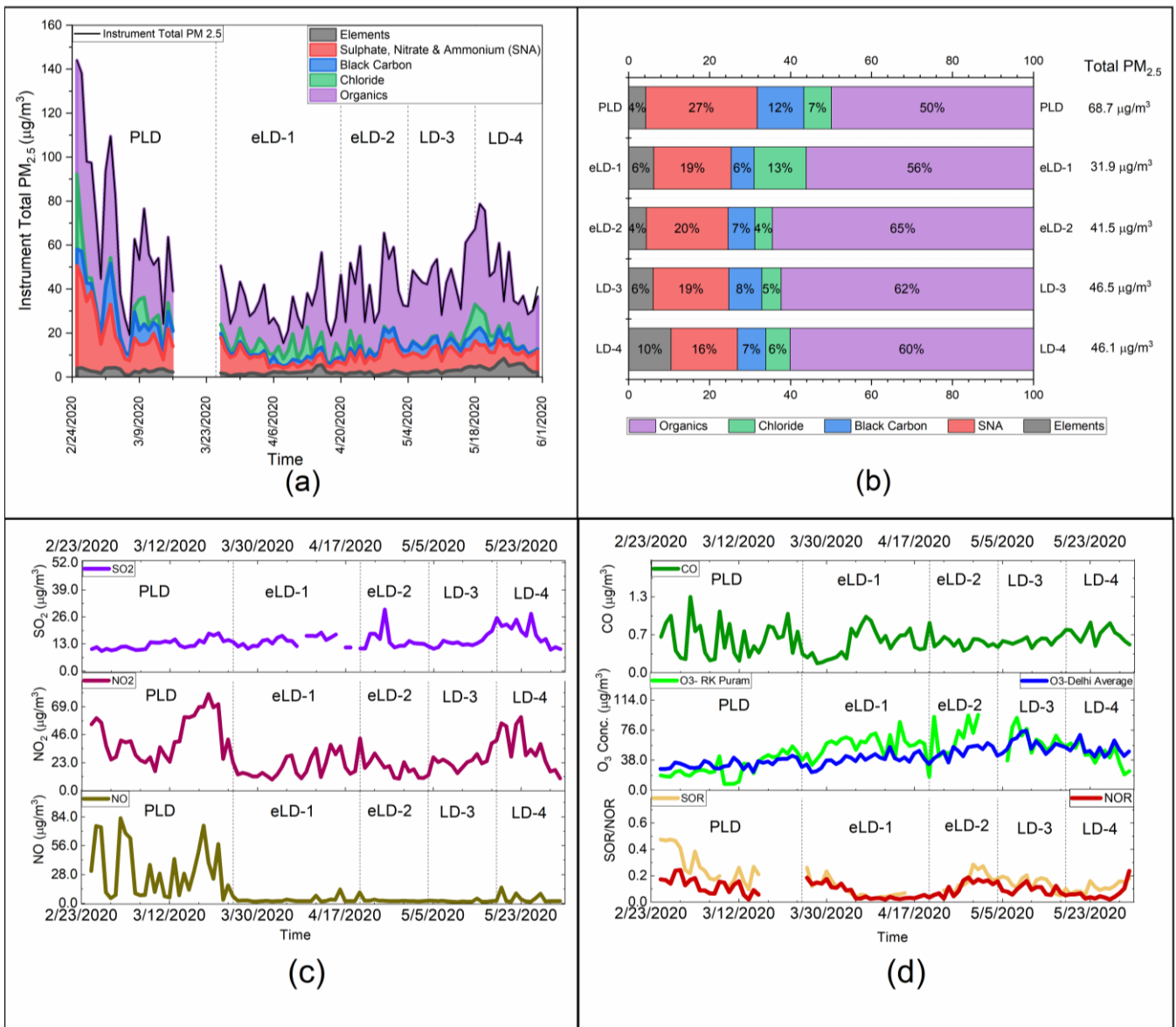


Figure 1: Effect of the lockdown on gaseous pollutants and particulate matter, (a) Time variation of instrument total PM_{2.5} and its major constituents; (b) Phase-wise composition of measured PM_{2.5}; (c) Time variation of SO₂, NO₂, NO (top to bottom); (d) Time variation of CO, O₃ (at RK Puram and average for Delhi), SOR and NOR (top to bottom)

In Figure 1 (d), we also note that the behavior of O₃ doesn't reconcile with the trend followed by total PM_{2.5} and other gaseous pollutants discussed above and are found to increase by 98%, 121%, 118%, and 54% in each of eLD-1 to LD-4 w.r.t the PLD concentrations (Figure S6(a)). Similar, anomalies in terms of increase in ozone concentration following the lockdown have been observed in some recent studies, not only in India but also in different parts of China, France, Italy, and Spain (Sicard et al., 2020; Tobías et al., 2020; Zheng et al., 2020) and have attributed the increase in ozone to the reduction of NO_x in a VOC-limited environment (Monks et al., 2015). This non-linear coupling between VOC, NO_x and O₃ was originally discussed in an early study by Finlayson-Pitts and Pitts (1993). However, it is also interesting to note that despite the increasing NO_x concentrations in LD-4 and high O₃ concentrations during the same period NOR remains 0.06, indicating low concentrations of particulate nitrate. The same scenario has been discussed by Finlayson-Pitts and Pitts (1993), presenting the hypothesis that VOC and NO_x compete for OH radical for oxidation. When the VOC to NO_x ratio increases (decreasing NO_x at constant VOC) the oxidation of VOC is favored over NO_x resulting in lower nitrate concentrations. Similarly, for SO₂ and associated lower sulfate indicated by low SOR despite high O₃, gas phase oxidation of SO₂, similar to NO₂ competes for the OH radical, while aqueous phase oxidation of SO₂ is limited by the acidity of the reaction products, as this oxidation route is efficient only near neutral conditions (Wilson et al., 1972). Further discussion on the variation of PM_{2.5}, its constituents, and gaseous pollutants is presented in SI section S3.1.

3.1 Source Apportionment of elemental PM_{2.5} (measured using Xact 625i)

The elements measured using the Xact 625i were subjected to source apportionment using PMF. A seven-factor solution was found to best represent the input data. The sources corresponding to the apportioned factors were assessed based on the species dominating every factor profile. Each of the species was quantified in two ways:

- a) Based on the percentage of factor mass, given by the average concentration of the species of interest divided by the sum of the average concentration of each species within the factor
- b) Based on percentage species across factors, given by the concentration of the species of interest in the factor under consideration divided by the sum of the concentration of the same species across all factors.

A detailed description of the resolved seven-factor solution (Figure 2) is as follows:

3.1.1 Vehicular Emissions

The vehicular emissions factor (Figure 2(a)) was found to be dominated by S (36%) in terms of the % factor mass, followed by Cl (19%), K (17%), Fe (13%), Ca (7%) and Zn (6%) respectively in terms of the percentage factor mass.

However, in terms of the percentage species across factors, vehicular emissions accounted for 60% of the total Mn content, followed by 33% of Ba, 30% of V, 22% of Zn, 15% of Ca, 13% of K, and 11% of S.

Sulfur and Vanadium is known to occur naturally in crude oil, while pollution control measures have remained focused on reducing sulfur content in fuels, studies have pointed out the use of sulfur in engine oil anti-wear additives (Fitch, 2019). Multiple studies in the past have attributed Mn, Fe, Zn, and Ba to vehicular emissions, brake wear, and engine wear, in particular, recognizing them as abundant trace elements in brake pads and brake lining (Gianini et al., 2012; Grigoratos and Martini, 2015; Rai et al., 2020b; Thorpe and Harrison, 2008). Ti and V have also been attributed to brake and tire wear in some studies in the past (Gerlofs-Nijland et al., 2019). Potassium is noted to be used as an anti-freeze inhibitor and as an additive in engine oils. Also, K is known to be present in all unleaded fuels (Spencer et al., 2006). Calcium and Chlorine are known to be added to engine lubricants, Ca-compounds serves as a base to neutralize acids, while Cl-based additives act as dispersants, to retain dirt in suspension, to protect the engine (Dyke et al., 2007; Lyyräinen et al., 1999; Rudnick, 2017).

In terms of the time variation (Figure S3(a)), this factor is significantly affected by the lockdown with a 96% reduction in average concentration from PLD to eLD-1 (Figure S6(b)), the time series and the composition pie-chart (Figure 2(b)) show a steady rise in the concentration of this factor, while the factor concentration in phase-4 remains 70% lower than its pre-lockdown value.

As an additional proxy, mobility trends (Google LLC, 2020) (Figure 2(c)) quantifying the percentage change in transit station mobility w.r.t PLD, was compared with the time variation of this factor, and a significant correlation (Pearson R = 0.81) between the two was noted.

In addition to the characteristic species noted above, this factor displayed a sharp diurnal peak coinciding with the morning rush hour and evening rush hour (Figure S4) during PLD and LD-4, when there was comparatively normal traffic load. During eLD-1 to LD-3, the vehicular movement has remained extremely restricted; thus, no diurnality in traffic-related emissions was found.

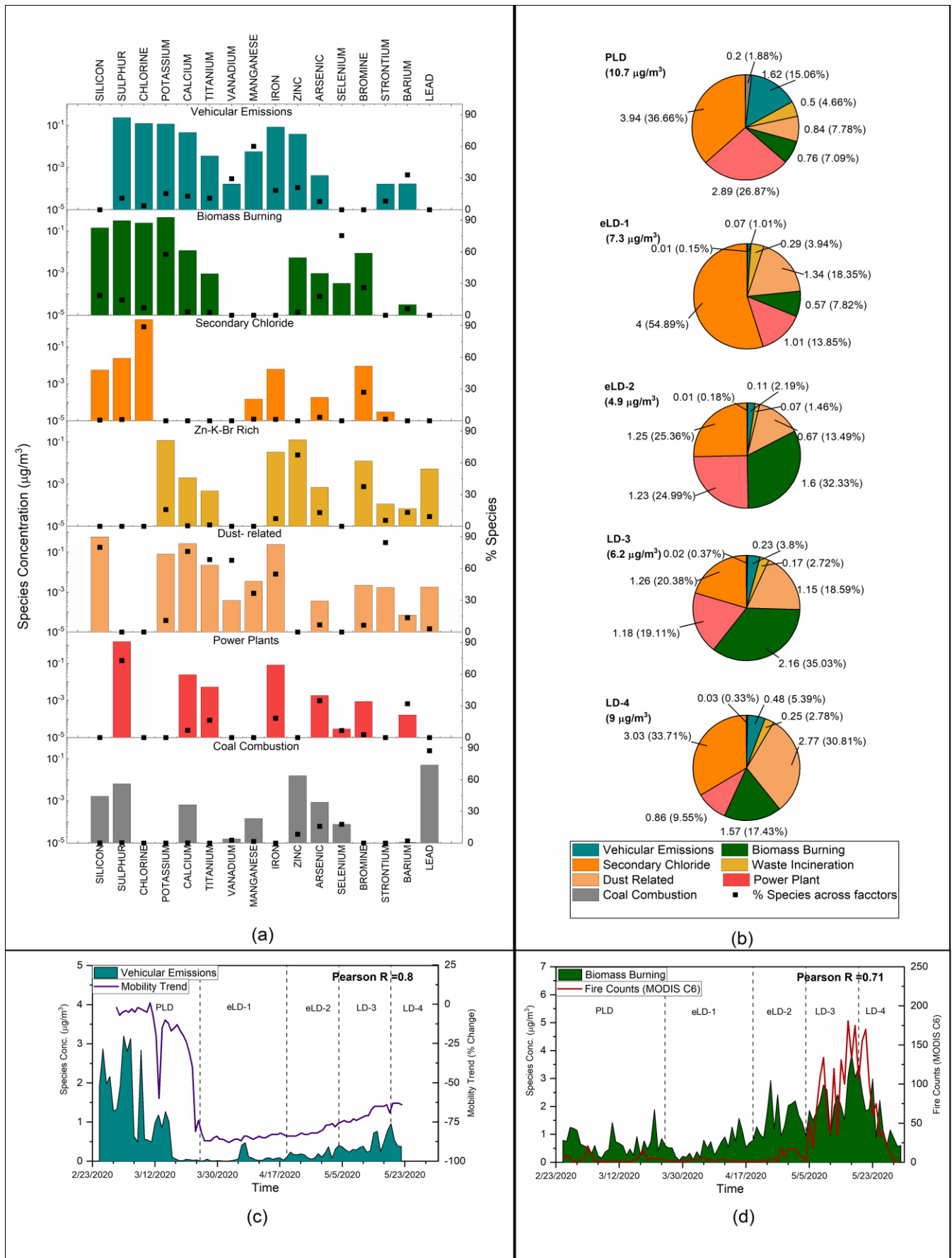


Figure 2: Source apportionment results for elemental particulate matter: (a) resolved source/factor profiles; (b) phase-wise contribution of each factor to total elemental fraction of $\text{PM}_{2.5}$; (c) Correlation of vehicular emissions with mobility trends (d) Correlation of biomass burning with fire counts

3.1.2 Biomass Burning

In terms of the % factor mass, the biomass burning factor (Figure 2(a)) was dominated by K (36%), followed by S (27%), Cl (21%), and Si (12%), respectively. Looking into the percentage species across factors biomass burning was found accountable for 75% of the total Se content, followed by 58% of K, 19% of Si, and 14% of S.

Multiple studies across the globe have proposed the use of potassium as an elemental marker to identify biomass source profiles (Khare and Baruah, 2010; Pant and Harrison, 2012; Reche et al., 2012; Shridhar et al., 2010). Past studies have also reported Se to reach significant levels in biomass grown in selenium-rich soils (Goldstein, 2018), which in turn are common in northern India (Sharma et al., 2009). Silicon is known to be emitted from the pyrolysis of fibers in biomass like straw, cereal, and grass (Oberberger et al., 2006). Li et al. (2003) concluded that for fresh biomass burning plumes, most potassium exists as KCl, while in aged plumes, the chlorides are partly replaced by sulfates—thus providing evidence for high sulfur and chloride concentrations in conjunction with potassium in biomass associated source inventories.

The average factor concentration is found to lower by 25% in eLD-1 (Figure S6(b)); however, that may be a direct consequence of lower biomass burning emissions. Again it is not instinctive to assume any strong dependence of the lockdown event over biomass burning emissions. Thus it is difficult to ascertain whether the decrease in the concentration stemmed from the lockdown. The concentration starts increasing in April and peak in May, which also coincides with the wheat harvesting season, thus resulting in increased residual crop burning activities (Jethva et al., 2019). The factor time series was also compared with satellite-based fire counts (LANCER FIRMS, 2020) in a 200 km radius of the sampling site (Figure 2(d)), and a significant correlation (Pearson $R = 0.71$) was observed between them.

3.1.3 Secondary Chloride

The Secondary Chloride factor (Figure 2(a)) is solely dominated by chlorine in terms of factor mass, with Cl accounting for 98% of the factor mass. Also, in terms of % species across factors, secondary chloride contributes to 89% of total measured Cl and 27% of total Br.

The diurnal variation associated with this factor (Figure S4) is very similar to that of NH_4 , with a sharp peak around 6:00 IST. This leads us to the possibility of this factor to stem from ammonium chloride. With lower saturation vapor pressure, ambient ammonia and HCl may condense in the particulate phase and vaporize back with an increase in saturation vapor pressure after sunrise.

A similar factor from source apportionment of PM₁ in Delhi was observed by Jaiprakash et al. (2017) It was suggested that HCl fumes transported from metal processing plants to the north-west of Delhi reacted with the high ammonia concentrations in Delhi to condense in the particulate phase (Warner et al., 2017). Similar conclusions were reached upon by Gani et al. (2019) for the high particulate chloride concentrations observed by them.

The secondary chloride factor seems to have no dependence on the lockdown event as the average concentration of this factor increases marginally from PLD to eLD-1 ($3.94 \mu\text{g}/\text{m}^3$ to $4 \mu\text{g}/\text{m}^3$) (Figure 2(b)).

From Figure S3(a), secondary chloride time series, we can note that almost all peaks for this factor correspond to a local wind direction in the sector of 302-333 degrees or NW direction. Also, the factor concentration is found to decrease noticeably in eLD-2 ($1.25 \mu\text{g}/\text{m}^3$) and remain low in LD-3 ($1.26 \mu\text{g}/\text{m}^3$) (Figure 2(b)). This again seems to have a dependence on the wind direction, starting from the beginning of eLD-2 up till the middle of LD-3, a shift in wind direction towards the southeast, can be noted. However, the wind direction again shifts to the northwest towards the end of phase-3, which marks the rise in the secondary chloride concentrations again.

The possible sources of Cl or Br emissions may include a variety of sources like waste burning or industries, however, to account for the lack of dependence of this factor on the lockdown and following relaxations, the source of HCl/HBr must also remain unaffected/minimally affected by the lockdown.

3.1.4 Zn-K-Br Rich

In terms of % factor mass, this factor is mainly composed of Zn (42%), K (40%), and Fe (11%). However, in terms of % species across factors, these factors contribute to 68% of total Zn, 38% of total Br, and 16% of K (Figure 2(a)).

Multiple studies in the past have attributed a Zn-dominated factor to waste incineration (Gupta et al., 2012; Julander et al., 2014; Parekh et al., 1967; Sweet et al., 1993). These studies have mainly been associated with electronic or municipal waste burning, where a halide catalyzes the volatilization of metals to form metal halogenides, usual metals related to waste incineration in addition to Zn, include K, As, Fe and Pb. While Cl is a more abundant halide, but Vehlow et al. (2003) have discussed how Br may be high in plastics containing flame retardants and, in turn, drive the volatilization of heavy metals like Zn Fe and As. However, Zn and As have also been attributed to iron/steel industries and waste incineration (Duan and Tan, 2013). Also, past studies have attributed Zn-Pb-Cl to industrial emissions (Bullock and Gregory, 1991).

This ambiguity in the published literature regarding tracer for waste incineration/industrial activities has to lead us to define this factor as a Zn-K-Br rich factor only. In terms of the time variation (Figure S3(a)) the factor in line with total

PM_{2.5} decreases by 42% in eLD-1 w.r.t pre-lockdown, followed by 85%, 54%, and 50% in each of eLD-2 to LD-4 w.r.t PLD concentrations (Figure S6(b)).

3.1.5 Dust Related

The predicted dust-related source profile (Figure 2(a)) is dominated by Si, accounting for 48% of the factor mass, followed by 22% and 20% of the factor mass for Ca and Fe, respectively. In terms of % species across factors, dust-related source accounts for 84% of total Sr, 80% of total Si, 76% of Ca, 68% each of Ti and V, 55% of Fe and 37% of Mn. Each of the above-noted species has been extensively used as tracers for road dust/crustal elements in multiple studies across the globe (Gupta et al., 2007; Kothai et al., 2011; Rai et al., 2020a; Sharma et al., 2016; Sun et al., 2019).

In terms of the time variation (Figure S3(a)) of this factor, there seems to be no observable effect of the lockdown on dust-related particulate matter. However, we observe a significant correlation of the factor concentration with ambient temperature (Pearson R= 0.64) (Figure S2(a)) and an inverse correlation with RH (Pearson R= -0.67) (Figure S2(a)), which is in agreement with several past studies (Csavina et al., 2014; Jayamurugan et al., 2013). Also, during LD-4, we observe an increase in the average concentration of this factor, from 1.15 $\mu\text{g}/\text{m}^3$ in LD-3 to 2.77 $\mu\text{g}/\text{m}^3$ in LD-4 (Figure 2(b)), which may be influenced by multiple meteorological parameters like WD, WS or gust events.

3.1.6 Power Plants

Considering the % factor mass, sulfur solely dominates this factor profile accounting for 93% of the total factor mass. In terms of the % species across the factors, the power plants factor contributes to 73% of the total sulfur, 35 % of As, and 32% of total Ba (Figure 2(a)).

In this study, the power plants factor (Figure S3(a)) displays a significant correlation with the SOR (Figure 1(d)) (Pearson R = 0.922), signaling towards the sulfur content in the particulate phase is actually in the form of aqueous sulfate. Also, past studies evaluating power plant emissions as well as source apportionment studies have highlighted the use of As and Ba as tracers for coal-based power plant emissions (Reddy et al., 2005; Zhao et al., 2017; Zoller et al., 1974).

Observing the time series of this factor, we do note a 65% decrease in eLD-1 w.r.t the PLD concentrations (Figure S6(b)). A recent report from the Power System Operation Corporation (POSOCO, 2020) does indicate a significant reduction (44% reduction in April compared to last year) in the power demand due to the closure or scaled-down operations in almost all industries due to the lockdown, which in turn could lead to temporarily scaled down operations

at some power plants. Thus, some order of reduction in source emission can also be partially responsible for the significant drop observed in the factor concentration at the receptor.

However, it would be implausible to attribute the entire reduction to the lockdown alone, as there has been significant variation in the factor concentration within the PLD (-54% to +89% w.r.t PLD average) (Figure S6(b)), indicating some role of metrological or other transport variables rather than the source emission alone for the variation in the concentration. Again, during eLD-2, the average concentration is found to increase relative to PLD levels; however, the concentration again starts to fall during LD-3 and LD-4, thus advising of some external metrological/transport phenomena affecting the concentration values.

3.1.7 Coal Combustion

The coal combustion factor (Figure 2(a)) is dominated by Lead, Zinc, and Sulfur accounting for 66%, 21%, and 8.5% of the total factor mass, respectively. Considering the % Species across factors, coal combustion is responsible for 87% of Pb, 18% of Se, 16% of As, and 9% of Zn. While coal combustion is found to account for only 0.3% of total sulfur, it is essential to note that the % contribution of this factor to elemental PM_{2.5} has remained quite low (less than 1.9%) throughout the study period.

As and Se have been widely used as markers for coal combustion (Gupta et al., 2007; Hien et al., 2001; Lee et al., 2008; Sharma et al., 2007). Zn again has been used as a marker for coal combustion in India, due to relatively higher Zn content in Indian coals (Almeida et al., 2006). While commercially available coal has lower Pb content, Negi et al. (1967) reported the higher concentrations of Pb and Zn in domestic soft coal. It is also important to note that domestic Indian coals have been found to have low sulfur content (less than 0.6% by mass) with an exception to coal deposits in north-eastern India with high sulfur content (Chandra, A, and Chandra, 2004; Sarkar, 2009). Also, past studies have reported Indian power plants to utilize blends of imported and domestic coals supporting the higher sulfate emissions from power plants (Central Electricity Authority, 2012; Chandra, A, and Chandra, 2004).

Evaluating the temporal variation associated with this factor (Figure S3(a)), we notice that the lockdown implementation brings about a 95% reduction in the average concentration of the coal combustion source, comparing eLD-1 to PLD conditions. With increasing relaxations, the percentage reduction in average concentration w.r.t the PLD falls to 90% in eLD-2 and LD-3 and finally 85% in LD-4 (Figure S6(b)).

Since the source profiles and supporting literature indicate domestic soft coal burning, the real-world sources may be connected to small scale industrial setups, eateries or household usage of domestic grade coal, and such sources appear to be drastically affected by the lockdown and display only a marginal increase in emissions even with increasing

relaxations. Such a variation could possibly stem from the massive outflow of migrant laborers from the NCT region, resulting in the sudden downfall of domestic coal usage for cooking purposes (Roy and Agarwal, 2020).

3.2 Source Apportionment of Organic Aerosols (measured using Q-ACSM)

The organic content of the total PM_{2.5} mass is subjected to source apportionment using PMF. A six-factor solution was found to fit the input data best. The apportioned factors were identified by the mass spectra signatures, their correlation with tracers, and their diurnal behavior (Ulbrich et al., 2009; Zhang et al., 2005b). The present study further correlates each apportioned factor to corresponding reference factor profiles from Ng et al. (2011). Figure 3 presents the predicted mass spectra for each profile, along with their temporal variation and correlation with external markers. The detailed description of each predicted source profile is as follows:

3.2.1 Semi-Volatile Oxygenated Organic Aerosol (SVOOA)

The factor profile, as seen in Figure 3(a), is characterized by a significant peak at m/z 43, which is a characteristic of less oxidized secondary organic aerosol (Li et al., 2019; Zhu et al., 2018). The diurnal variation (Figure S5) of this factor presents two peaks: early morning (6:00 – 9:00 IST) and a weaker peak at midnight, signaling SVOOA concentrations to be affected by photo-oxidation of fresh emissions (morning peak) along with boundary layer height (midnight peak), similar to observations made by Chakraborty et al. (2018). The SVOOA source profile predicted from the PMF analysis was noted to have a Pearson R correlation of 0.93 with the reference SVOOA profile from Ng et al. (2011)

The SVOOA factor time series displayed a strong correlation with NO₃ (measured using ACSM) (Pearson R = 0.95) (Figure 3(c)), which is in agreement with the trend reported in past studies (DeCarlo et al., 2010; Dzepina et al., 2009; Volkamer et al., 2006), and is attributed to the analogous semi-volatility of SVOOA and nitrate resulting in similar gas-particle partitioning.

The SVOOA factor drops significantly (86%) after the lockdown is implemented; the emissions increase with increased relaxations from eLD-2 to LD-3, however, there is a small drop (18%) in average concentration again from LD-3 to LD-4 (Figure S6(c)).

3.2.2 Hydrocarbon-like Organic Aerosol (HOA)

Alkyl fragment signatures distinctly mark this factor profile (Figure 3(a)) with prominent contributions from m/z 55 and 57 (Aiken et al., 2009; Ng et al., 2011). The resultant HOA profile has a strong correlation (Pearson R = 0.95) with reference HOA spectra from Ng et al. (2011).

Past studies have found HOA to correlate well with black carbon (BC) (Mohr et al., 2009; Sun et al., 2016). In the present study, we note an excellent correlation between BC and HOA (Pearson $R = 0.96$) (Figure 3(c)), during the PLD phase; however, post-lockdown the trend of BC and HOA become completely disparate, resulting in a negligible correlation between the two. The significant correlation with BC often is taken as support for the vehicular origin of HOA (DeWitt et al., 2015).

However, from section 3.1.1, we note the vehicular emissions to drop significantly post-lockdown (96%) while, HOA concentrations lower only by 14% post-lockdown. At the same time, it departs from the trend followed by BC (Figure 2(d)), indicating that during the lockdown, HOA originates from a source other than vehicular emissions.

The initial studies that looked into the deconvolution of HOA from POA (Zhang et al., 2005a) suggested its connection to vehicular origin based on the significant correlation with vehicular markers like NO_x and BC and the fine mode of particulate matter corresponding m/z 55 and 57 as compared to m/z 44 which grows larger while aging. Zhang et al. (2005a) also discussed car-chaser and lab-based studies, wherein both diesel emissions and lubricant combustion resulted in HOA like spectra, as heavy oils, lubricants, cooking oils are known to correspond to m/z 55, while mass spectra associated with gasoline and diesel-like fuels displayed a more definite m/z 57 peaks.

Hao et al. (2014) also observed appreciable HOA contributions in a low-traffic village setting. They attributed the source to be a combination of industrial, cooking, and biomass burning along with the low contribution from traffic.

Thus, it may be hypothesized that either HOA during the lockdown originates from diesel/lubricant based emissions from sources other than vehicles, like diesel-based generators in industries or cooking-related activities. However, similar to SVOOA, even HOA experiences a sharp reduction towards the end of LD-4.

3.2.3 Biomass Burning Organic Aerosol (BBOA-1 and BBOA-2)

In the present study, we resolve two separate biomass burning related factors (Figure 3(a)). However, BBOA-1 can be categorized as a fresh/ primary emission, with its mass spectra highly correlated to the BBOA profile from Ng et al. (2011) (Pearson $R = 0.937$). For the other BBOA profile, i.e., BBOA-2, we observe enhanced concentrations of m/z 43 and m/z 44, indicating that BBOA-2 is relatively aged. Also, the diurnal variation (Figure S5) associated with BBOA-1 displays primary emission like behavior, with early morning peaks, while BBOA-2 also displays peaks around noon, which is a characteristic of m/z 44 or CO_2^+ , indicating the possibility of regionally transported emissions responsible for BBOA-2.

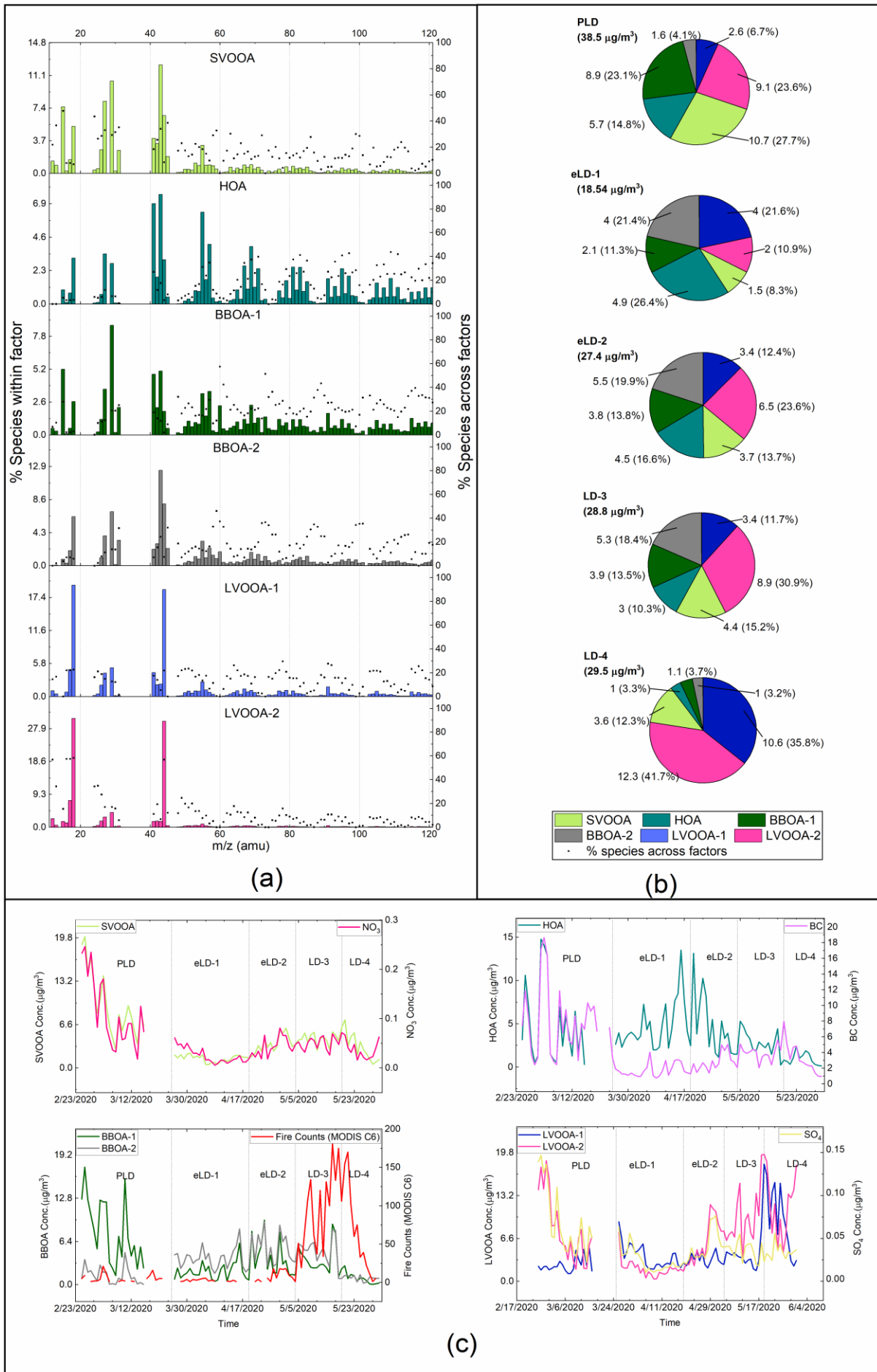


Figure 3: Source apportionment results for organic particulate matter: (a) resolved source/factor profiles; (b) phase-wise contribution of each factor to total organic aerosol; (c) correlation of factors with external markers

BBOA-2 also shares a good correlation with the Ng et al. (2011), reference BBOA profile (Pearson R =0.82). Both BBOA-1 and BBOA-2 are marked by intensified peaks corresponding to m/z 60. Levoglucosan is known to be proportional to $C_2H_4O_2^+$ (a fragment at m/z 60) is extensively used as a marker for biomass burning in AMS based studies (Aiken et al., 2009).

Similar to the biomass burning factor in section 3.1, it is not intuitive to presume an effect of the lockdown on biomass burning. However, comparing the two BBOA factors, we see that BBOA-1 displays higher concentrations in pre-lockdown, while reduced order (76%) values following lockdown, steadily rising from eLD-1 to LD-3. BBOA-2 displays lower concentrations in the PLD period and steadily rise to a maxima ($5.1\mu g/m^3$) up till LD-3 (Figure 3(b)). Thus, indicating that while the lockdown leads to a decrease in the primary BBOA emissions (BBOA-1), it in some way enhances the regional transported/aged fraction of BBOA (BBOA-2). However, similar to both SVOOA and HOA, both BBOA factors significantly reduce both in absolute concentration and percentage contribution in LD-4 (Figure S3(b) & Figure 3(b)).

Interestingly none of the BBOA factors display any positive correlation or similar trend with the satellite-based fire counts (LANCIE FIRMS, 2020) (Figure 3(c)), which was seen in the potassium dominated biomass burning factor in section 3.1.

A study by Brown et al. (2016) can aid in the reason behind such discrepancy. They studied the comparison between different biomass burning markers like K^+ , BC, and Levoglucosan or in turn m/z 60. It was noted that K^+ and BC are more prominent products in flaming combustion (which is usually captured as fire counts). However, Levoglucosan is a more prominent emission in the case of smoldering combustion (Lee et al., 2010).

3.2.4 Low Volatile Oxygenated Organic Aerosol (LVOOA-1 and LVOOA-2)

LVOOA is addressed as an aged or oxidized aerosol and is majorly marked by a distinct peak of m/z 44 or CO_2^+ . In this study, we resolve two LVOOA factors (Figure 3(a)), i.e., LVOOA-1 and LVOOA-2. Both the LVOOA factors display a strong correlation with the Ng et al. (2011) reference spectra (Pearson R =0.95, 0.93 for LVOOA-1, and LVOOA-2, respectively).

Observing the temporal variation, we see that LVOOA-2 is at a high concentration ($9.1\mu g/m^3$), which reduces after the lockdown ($2\mu g/m^3$) and steadily rises to a noticeably high concentration in LD-4 ($12.3\mu g/m^3$). On the other hand, LVOOA-1 mostly remains at a lower concentration from PLD to LD-3 (from $2\mu g/m^3$ to $4\mu g/m^3$); however, it rises to

a significant concentration in LD-4 ($10.6 \mu\text{g}/\text{m}^3$) (Figure 3(b)). It is important to note that all apportioned organic factors decrease considerably in LD-4, while both the LVOOA factors experience a significant rise.

LVOOA is known to correlate well with sulfate, citing the similar low-volatility observed in both species (Zhu et al., 2018). In Figure 3(c) we see that LVOOA-1 neither follows the trend nor is correlated to sulfate, whereas LVOOA-2 expresses a significant correlation with sulfate (measured using ACSM) during PLD (Pearson $R = 0.93$), and continues to display a significant correlation up till LD-3 (Pearson $R = 0.69$); however, the correlation significantly deteriorates in LD-4.

Investigating the diurnal variations associated with both factors (Figure S5), we see that LVOOA-2 displays a flat diurnal profile with a marginal peak at noon, which is characteristic of CO_2^+ formation by photochemical oxidation. However, if we look at the phase-wise diurnal variation, the diurnal profile for LVOOA-1 in lockdown phase-4 behaves like a primary pollutant diurnal with an early morning peak rather than the afternoon peak, suggesting primary aerosol-like formation mechanism for LVOOA-1.

Earlier in section 3, we noted low SOR and NOR values, which usually correspond to primary rather than secondary aerosols. We must also take into account that LD-4 began right after the period when ozone had reached its peak concentrations (section 3.1.2).

All these facts taken collectively indicate that in some way, all primary and intermediate organic aerosols are chemically aged in presence on high O_3 to form LVOOA, leading to a reduction in all other organic factors and a significant rise in LVOOA. Jimenez et al. (2009), on a similar note, stated that the atmospheric oxidation of organic aerosol (OA) converges to LVOOA regardless of the original OA source. However, it is also important to note that the diurnal variation of LVOOA-1 hinted towards its primary emissions. Another study by Liggio and Li (2013), suggested a mechanism for the formation of oxygenated primary organic aerosols by uptake of primary oxygenated organic gases to aerosols, and thus presents a possible explanation for the primary rather than secondary origin of LVOOA-1.

4. Conclusions

The COVID-19 lockdown resulted in an unprecedented decline in anthropogenic activities, which in turn led to a considerable reduction ($\sim 54\%$) in ambient $\text{PM}_{2.5}$ levels. The detailed source apportionment results presented in this study reveal the varying impact of the lockdown on different sources contributing to the elemental and organic fractions of $\text{PM}_{2.5}$. Source apportionment of elemental $\text{PM}_{2.5}$ yielded seven source profiles; the vehicular emissions, coal combustion, and Zn-K-Br rich sources were severely impacted by the lockdown. However, the lockdown seemed to

have minimal or no impact on biomass burning and dust-related sources. The dust-related factor displayed dependence on meteorological factors, while increased biomass burning emissions coincided with the crop burning season. The power plants-related elemental PM seems to be affected by both the lockdown and meteorological parameters. Interestingly, the secondary chloride factor observed elevated concentration peaks majorly from the north-west direction, and remained largely unaffected by the lockdown.

The organics-only PMF resulted in 6 factors, i.e., SVOOA, HOA, two BBOA, and two LVOOA factors. The lockdown seems to have an appreciable effect on SVOOA factor concentrations with a reduction (86%) in eLD-1, followed by increased concentrations with relaxations in the lockdown. The fresh BBOA emissions (BBOA-1) decline following the lockdown, while the aged BBOA emissions (BBOA-2) rise, signaling intensified transport of BBOA related emissions from regional sources following the lockdown. HOA concentrations were marginally affected by the lockdown indicating sources other than vehicular emissions played a dominant role in HOA related emissions, contrary to the belief of HOA being dominated by vehicular emissions. The organic aerosol (OA) source apportionment also highlights a sharp rise in the LVOOA concentrations in LD-4 accompanied by a concomitant decay in concentrations of all other resolved OA sources, this rise is attributed to the oxidation of primary OA due to high ozone concentrations.

This is the first study to quantify the impact of the COVID-induced lockdown on highly time-resolved sources of ambient PM_{2.5} in India. These results have important implications for guiding future policies targeted and decreasing PM levels in not only Delhi but the entire IGP, so that the actions are targeted on actual sources of emission, knowing the level of impact a particular source has on total PM levels. The results also highlight a prime concern for driving future emission control strategies, especially upcoming vehicular emission standards like Bharat Stage 6 (BS-VI), which may realize the low NO_x, VOC-limited setting without a lockdown, and lead to an inadvertent rise in ozone and LVOOA.

Acknowledgments

The authors would like to acknowledge the IRD Grand Challenge Project grant, IIT Delhi (Grant No. IITD/IRD/MI01810G), for the funding support to carry out this project.

CRedit author statement:

Chirag Manchanda: Methodology, Software, Formal Analysis, Writing - Original Draft, Investigation, Visualization.

Mayank Kumar: Conceptualization, Methodology, Writing - Review & Editing, Supervision, Resources, Project Administration, Funding Acquisition. **Vikram Singh:** Methodology, Writing - Review & Editing, Supervision,

Resources, Funding Acquisition. **Mohd. Faisal:** Formal Analysis, Investigation, Data Curation. **Naba Hazarika:** Data

Curation, Investigation. **Ashutosh Shukla**: Validation, Writing - Review & Editing. **Vipul Lalchandani**: Validation, Writing - Review & Editing. **Vikas Goel**: Investigation, Data Curation. **Navaneeth Thamban**: Validation. **Dilip Ganguly**: Resources, Data Curation. **Sachchida Nand Tripathi**: Conceptualization, Methodology, Supervision, Resources, Project Administration

References

- Aiken, A.C., Salcedo, D., Cubison, M.J., Huffman, J.A., DeCarlo, P.F., Ulbrich, I.M., Docherty, K.S., Sueper, D., Kimmel, J.R., Worsnop, D.R., Trimborn, A., Northway, M., Stone, E.A., Schauer, J.J., Volkamer, R.M., Fortner, E., de Foy, B., Wang, J., Laskin, A., Shutthanandan, V., Zheng, J., Zhang, R., Gaffney, J., Marley, N.A., Paredes-Miranda, G., Arnott, W.P., Molina, L.T., Sosa, G., Jimenez, J.L., 2009. Mexico City aerosol analysis during MILAGRO using high resolution aerosol mass spectrometry at the urban supersite (T0) – Part 1: Fine particle composition and organic source apportionment. *Atmos. Chem. Phys.* 9, 6633–6653.
<https://doi.org/10.5194/acp-9-6633-2009>
- Almeida, S.M., Pio, C.A., Freitas, M.C., Reis, M.A., Trancoso, M.A., 2006. Source apportionment of atmospheric urban aerosol based on weekdays/weekend variability: evaluation of road re-suspended dust contribution. *Atmos. Environ.* 40, 2058–2067. <https://doi.org/10.1016/j.atmosenv.2005.11.046>
- Bao, R., Zhang, A., 2020. Does lockdown reduce air pollution? Evidence from 44 cities in northern China. *Sci. Total Environ.* 731, 139052. <https://doi.org/10.1016/j.scitotenv.2020.139052>
- Brown, S., Lee, T., Roberts, P., Collett, J., 2016. Wintertime Residential Biomass Burning in Las Vegas, Nevada; Marker Components and Apportionment Methods. *Atmosphere (Basel)*. 7, 58.
<https://doi.org/10.3390/atmos7040058>
- Bullock, P., Gregory, P.J., 1991. Soils: A Neglected Resource in Urban Areas, in: *Soils in the Urban Environment*. Blackwell Publishing Ltd., Oxford, UK, pp. 1–4. <https://doi.org/10.1002/9781444310603.ch1>
- Burr, M.J., Zhang, Y., 2011. Source apportionment of fine particulate matter over the Eastern U.S. Part I: source sensitivity simulations using CMAQ with the Brute Force method. *Atmos. Pollut. Res.* 2, 300–317.
<https://doi.org/10.5094/APR.2011.036>
- Central Electricity Authority, 2012. Report of The Group for Studying Range of Blending of Imported Coal with Domestic Coal. New Delhi.

- Chakraborty, A., Mandariya, A.K., Chakraborti, R., Gupta, T., Tripathi, S.N., 2018. Realtime chemical characterization of post monsoon organic aerosols in a polluted urban city: Sources, composition, and comparison with other seasons. *Environ. Pollut.* 232, 310–321. <https://doi.org/10.1016/j.envpol.2017.09.079>
- Chandra, A, and Chandra, H., 2004. Impact of Indian and imported coal on Indian thermal power plants. *J. Sci. Ind. Res. (India)*. 63, 156–162.
- Csavina, J., Field, J., Félix, O., Corral-Avitia, A.Y., Sáez, A.E., Betterton, E.A., 2014. Effect of wind speed and relative humidity on atmospheric dust concentrations in semi-arid climates. *Sci. Total Environ.* 487, 82–90. <https://doi.org/10.1016/j.scitotenv.2014.03.138>
- DeCarlo, P.F., Ulbrich, I.M., Crouse, J., de Foy, B., Dunlea, E.J., Aiken, A.C., Knapp, D., Weinheimer, A.J., Campos, T., Wennberg, P.O., Jimenez, J.L., 2010. Investigation of the sources and processing of organic aerosol over the Central Mexican Plateau from aircraft measurements during MILAGRO. *Atmos. Chem. Phys.* 10, 5257–5280. <https://doi.org/10.5194/acp-10-5257-2010>
- DeWitt, H.L., Hellebust, S., Temime-Roussel, B., Ravier, S., Polo, L., Jacob, V., Buisson, C., Charron, A., André, M., Pasquier, A., Besombes, J.L., Jaffrezo, J.L., Wortham, H., Marchand, N., 2015. Near-highway aerosol and gas-phase measurements in a high-diesel environment. *Atmos. Chem. Phys.* 15, 4373–4387. <https://doi.org/10.5194/acp-15-4373-2015>
- Duan, J., Tan, J., 2013. Atmospheric heavy metals and Arsenic in China: Situation, sources and control policies. *Atmos. Environ.* 74, 93–101. <https://doi.org/10.1016/j.atmosenv.2013.03.031>
- Dyke, P.H., Sutton, M., Wood, D., Marshall, J., 2007. Investigations on the effect of chlorine in lubricating oil and the presence of a diesel oxidation catalyst on PCDD/F releases from an internal combustion engine. *Chemosphere* 67, 1275–1286. <https://doi.org/10.1016/j.chemosphere.2006.12.010>
- Dzepina, K., Volkamer, R.M., Madronich, S., Tulet, P., Ulbrich, I.M., Zhang, Q., Cappa, C.D., Ziemann, P.J., Jimenez, J.L., 2009. Evaluation of recently-proposed secondary organic aerosol models for a case study in Mexico City. *Atmos. Chem. Phys.* 9, 5681–5709. <https://doi.org/10.5194/acp-9-5681-2009>
- Fehsenfeld, F., 2004. Chapter 5, in: Howard McMurry, P., F. Shepherd, M., S. Vickery, J. (Eds.), *Particulate Matter Science for Policy Makers: A NARSTO Assessment*. Cambridge University Press.
- Finlayson-Pitts, B.J., Pitts, J.N., 1993. *Atmospheric Chemistry of Tropospheric Ozone Formation: Scientific and Regulatory Implications*. *Air Waste* 43, 1091–1100. <https://doi.org/10.1080/1073161X.1993.10467187>

- Fitch, J., 2019. Copper and Your Diesel Engine Oils [WWW Document]. Mach. Lubr. Noria Corp. URL www.machinerylubrication.com/Read/646/copper-diesel-engine-oil
- Gani, S., Bhandari, S., Seraj, S., Wang, D.S., Patel, K., Soni, P., Arub, Z., Habib, G., Hildebrandt Ruiz, L., Apte, J.S., 2019. Submicron aerosol composition in the world's most polluted megacity: the Delhi Aerosol Supersite study. *Atmos. Chem. Phys.* 19, 6843–6859. <https://doi.org/10.5194/acp-19-6843-2019>
- Gerlofs-Nijland, M.E., Bokkers, B.G.H., Sachse, H., Reijnders, J.J.E., Gustafsson, M., Boere, A.J.F., Fokkens, P.F.H., Leseman, D.L.A.C., Augsburg, K., Cassee, F.R., 2019. Inhalation toxicity profiles of particulate matter: a comparison between brake wear with other sources of emission. *Inhal. Toxicol.* 31, 89–98. <https://doi.org/10.1080/08958378.2019.1606365>
- Gianini, M.F.D., Gehrig, R., Fischer, A., Ulrich, A., Wichser, A., Hueglin, C., 2012. Chemical composition of PM10 in Switzerland: An analysis for 2008/2009 and changes since 1998/1999. *Atmos. Environ.* 54, 97–106. <https://doi.org/10.1016/j.atmosenv.2012.02.037>
- Goldstein, I.S., 2018. *Organic Chemicals from Biomass*. CRC Press.
- Google LLC, 2020. Google COVID-19 Community Mobility Reports.
- Grigoratos, T., Martini, G., 2015. Brake wear particle emissions: a review. *Environ. Sci. Pollut. Res.* 22, 2491–2504. <https://doi.org/10.1007/s11356-014-3696-8>
- Gupta, A.K., Karar, K., Srivastava, A., 2007. Chemical mass balance source apportionment of PM10 and TSP in residential and industrial sites of an urban region of Kolkata, India. *J. Hazard. Mater.* 142, 279–287. <https://doi.org/10.1016/j.jhazmat.2006.08.013>
- Gupta, I., Salunkhe, A., Kumar, R., 2012. Source apportionment of PM10 by positive matrix factorization in urban area of Mumbai, India. *Sci. World J.* 2012. <https://doi.org/10.1100/2012/585791>
- Hao, L.Q., Kortelainen, A., Romakkaniemi, S., Portin, H., Jaatinen, A., Leskinen, A., Komppula, M., Miettinen, P., Sueper, D., Pajunoja, A., Smith, J.N., Lehtinen, K.E.J., Worsnop, D.R., Laaksonen, A., Virtanen, A., 2014. Atmospheric submicron aerosol composition and particulate organic nitrate formation in a boreal forestland–urban mixed region. *Atmos. Chem. Phys.* 14, 13483–13495. <https://doi.org/10.5194/acp-14-13483-2014>
- Hien, P.D., Binh, N.T., Truong, Y., Ngo, N.T., Sieu, L.N., 2001. Comparative receptor modelling study of TSP, PM2 and PM2-10 in Ho Chi Minh City. *Atmos. Environ.* 35, 2669–2678. <https://doi.org/10.1016/S1352->

- Jaiprakash, Singhai, A., Habib, G., Raman, R.S., Gupta, T., 2017. Chemical characterization of PM_{1.0} aerosol in Delhi and source apportionment using positive matrix factorization. *Environ. Sci. Pollut. Res.* 24, 445–462. <https://doi.org/10.1007/s11356-016-7708-8>
- Jayamurugan, R., Kumaravel, B., Palanivelraja, S., Chockalingam, M.P., 2013. Influence of Temperature, Relative Humidity and Seasonal Variability on Ambient Air Quality in a Coastal Urban Area. *Int. J. Atmos. Sci.* 2013, 1–7. <https://doi.org/10.1155/2013/264046>
- Jethva, H., Torres, O., Field, R.D., Lyapustin, A., Gautam, R., Kayetha, V., 2019. Connecting Crop Productivity, Residue Fires, and Air Quality over Northern India. *Sci. Rep.* 9. <https://doi.org/10.1038/s41598-019-52799-x>
- Jimenez, J.L., Canagaratna, M.R., Donahue, N.M., Prevot, A.S.H., Zhang, Q., Kroll, J.H., DeCarlo, P.F., Allan, J.D., Coe, H., Ng, N.L., Aiken, A.C., Docherty, K.S., Ulbrich, I.M., Grieshop, A.P., Robinson, A.L., Duplissy, J., Smith, J.D., Wilson, K.R., Lanz, V.A., Hueglin, C., Sun, Y.L., Tian, J., Laaksonen, A., Raatikainen, T., Rautiainen, J., Vaattovaara, P., Ehn, M., Kulmala, M., Tomlinson, J.M., Collins, D.R., Cubison, M.J., Dunlea, J., Huffman, J.A., Onasch, T.B., Alfarra, M.R., Williams, P.I., Bower, K., Kondo, Y., Schneider, J., Drewnick, F., Borrmann, S., Weimer, S., Demerjian, K., Salcedo, D., Cottrell, L., Griffin, R., Takami, A., Miyoshi, T., Hatakeyama, S., Shimojo, A., Sun, J.Y., Zhang, Y.M., Dzepina, K., Kimmel, J.R., Sueper, D., Jayne, J.T., Herndon, S.C., Trimborn, A.M., Williams, L.R., Wood, E.C., Middlebrook, A.M., Kolb, C.E., Baltensperger, U., Worsnop, D.R., 2009. Evolution of Organic Aerosols in the Atmosphere. *Science* (80-.). 326, 1525–1529. <https://doi.org/10.1126/science.1180353>
- Julander, A., Lundgren, L., Skare, L., Grandér, M., Palm, B., Vahter, M., Lidén, C., 2014. Formal recycling of e-waste leads to increased exposure to toxic metals: An occupational exposure study from Sweden. *Environ. Int.* 73, 243–251. <https://doi.org/10.1016/j.envint.2014.07.006>
- Khare, P., Baruah, B.P., 2010. Elemental characterization and source identification of PM_{2.5} using multivariate analysis at the suburban site of North-East India. *Atmos. Res.* 98, 148–162. <https://doi.org/10.1016/j.atmosres.2010.07.001>
- Kothai, P., Saradhi, I.V., Pandit, G.G., Markwitz, A., Puranik, V.D., 2011. Chemical Characterization and Source Identification of Particulate Matter at an Urban Site of Navi Mumbai, India. *Aerosol Air Qual. Res.* 11, 560–569. <https://doi.org/10.4209/aaqr.2011.02.0017>

- Kumari, P., Toshniwal, D., 2020. Impact of lockdown measures during COVID-19 on air quality– A case study of India. *Int. J. Environ. Health Res.* 00, 1–8. <https://doi.org/10.1080/09603123.2020.1778646>
- LANCE FIRMS, 2020. MODIS Collection 6 [WWW Document]. NASA’s Earth Sci. Data Inf. Syst. <https://doi.org/https://doi.org/10.5067/firms/modis/mcd14dl.nrt.006>
- Lee, S., Liu, W., Wang, Y., Russell, A.G., Edgerton, E.S., 2008. Source apportionment of PM_{2.5}: Comparing PMF and CMB results for four ambient monitoring sites in the southeastern United States. *Atmos. Environ.* 42, 4126–4137. <https://doi.org/10.1016/j.atmosenv.2008.01.025>
- Lee, T., Sullivan, A.P., Mack, L., Jimenez, J.L., Kreidenweis, S.M., Onasch, T.B., Worsnop, D.R., Malm, W., Wold, C.E., Hao, W.M., Collett, J.L., 2010. Chemical Smoke Marker Emissions During Flaming and Smoldering Phases of Laboratory Open Burning of Wildland Fuels. *Aerosol Sci. Technol.* 44, i–v. <https://doi.org/10.1080/02786826.2010.499884>
- Li, J., Liu, Q., Li, Y., Liu, T., Huang, D., Zheng, J., Zhu, W., Hu, M., Wu, Y., Lou, S., Hallquist, Å.M., Hallquist, M., Chan, C.K., Canonaco, F., Prévôt, A.S.H., Fung, J.C.H., Lau, A.K.H., Yu, J.Z., 2019. Characterization of Aerosol Aging Potentials at Suburban Sites in Northern and Southern China Utilizing a Potential Aerosol Mass (Go:PAM) Reactor and an Aerosol Mass Spectrometer. *J. Geophys. Res. Atmos.* 124, 5629–5649. <https://doi.org/10.1029/2018JD029904>
- Li, J., Pósfai, M., Hobbs, P. V., Buseck, P.R., 2003. Individual aerosol particles from biomass burning in southern Africa: 2, Compositions and aging of inorganic particles. *J. Geophys. Res. Atmos.* 108, n/a-n/a. <https://doi.org/10.1029/2002JD002310>
- Li, L., Li, Q., Huang, L., Wang, Q., Zhu, A., Xu, J., Liu, Ziyi, Li, H., Shi, L., Li, R., Azari, M., Wang, Y., Zhang, X., Liu, Zhiqiang, Zhu, Y., Zhang, K., Xue, S., Ooi, M.C.G., Zhang, D., Chan, A., 2020. Air quality changes during the COVID-19 lockdown over the Yangtze River Delta Region: An insight into the impact of human activity pattern changes on air pollution variation. *Sci. Total Environ.* 732. <https://doi.org/10.1016/j.scitotenv.2020.139282>
- Liggio, J., Li, S.M., 2013. A new source of oxygenated organic aerosol and oligomers. *Atmos. Chem. Phys.* 13, 2989–3002. <https://doi.org/10.5194/acp-13-2989-2013>
- Lv, Z., Wang, X., Deng, F., Ying, Q., Archibald, A.T., Jones, R.L., Ding, Y., Cheng, Y., Fu, M., Liu, Y., Man, H., Xue, Z., He, K., Hao, J., Liu, H., 2020. Significant reduced traffic in Beijing failed to relieve haze pollution

during the COVID-19 lockdown: implications for haze mitigation.

- Lyyränen, J., Jokiniemi, J., Kauppinen, E.I., Joutsensaari, J., 1999. Aerosol characterisation in medium-speed diesel engines operating with heavy fuel oils. *J. Aerosol Sci.* 30, 771–784. [https://doi.org/10.1016/S0021-8502\(98\)00763-0](https://doi.org/10.1016/S0021-8502(98)00763-0)
- Mahato, S., Pal, S., Ghosh, K.G., 2020. Effect of lockdown amid COVID-19 pandemic on air quality of the megacity Delhi, India. *Sci. Total Environ.* 730, 139086. <https://doi.org/10.1016/j.scitotenv.2020.139086>
- Mohr, C., Huffman, J.A., Cubison, M.J., Aiken, A.C., Docherty, K.S., Kimmel, J.R., Ulbrich, I.M., Hannigan, M., Jimenez, J.L., 2009. Characterization of Primary Organic Aerosol Emissions from Meat Cooking, Trash Burning, and Motor Vehicles with High-Resolution Aerosol Mass Spectrometry and Comparison with Ambient and Chamber Observations. *Environ. Sci. Technol.* 43, 2443–2449. <https://doi.org/10.1021/es8011518>
- Monks, P.S., Archibald, A.T., Colette, A., Cooper, O., Coyle, M., Derwent, R., Fowler, D., Granier, C., Law, K.S., Mills, G.E., Stevenson, D.S., Tarasova, O., Thouret, V., von Schneidmesser, E., Sommariva, R., Wild, O., Williams, M.L., 2015. Tropospheric ozone and its precursors from the urban to the global scale from air quality to short-lived climate forcer. *Atmos. Chem. Phys.* 15, 8889–8973. <https://doi.org/10.5194/acp-15-8889-2015>
- Negi, B., Sadasivan, S., Mishra, U., 1967. Aerosol composition and sources in Urban areas in India. *Atmos. Environ.* 21, 1259–1266. [https://doi.org/10.1016/0004-6981\(67\)90072-8](https://doi.org/10.1016/0004-6981(67)90072-8)
- Ng, N.L., Canagaratna, M.R., Jimenez, J.L., Chhabra, P.S., Seinfeld, J.H., Worsnop, D.R., 2011. Changes in organic aerosol composition with aging inferred from aerosol mass spectra. *Atmos. Chem. Phys.* 11, 6465–6474. <https://doi.org/10.5194/acp-11-6465-2011>
- Obernberger, I., Brunner, T., Bärnthaler, G., 2006. Chemical properties of solid biofuels-significance and impact. *Biomass and Bioenergy* 30, 973–982. <https://doi.org/10.1016/j.biombioe.2006.06.011>
- Ohta, S., Okita, T., 1990. A chemical characterization of atmospheric aerosol in Sapporo. *Atmos. Environ. Part A. Gen. Top.* 24, 815–822. [https://doi.org/10.1016/0960-1686\(90\)90282-R](https://doi.org/10.1016/0960-1686(90)90282-R)
- Paatero, P., 1999. The Multilinear Engine—A Table-Driven, Least Squares Program for Solving Multilinear Problems, Including the n -Way Parallel Factor Analysis Model. *J. Comput. Graph. Stat.* 8, 854–888. <https://doi.org/10.1080/10618600.1999.10474853>
- Paatero, P., 1997. Least squares formulation of robust non-negative factor analysis. *Chemom. Intell. Lab. Syst.* 37,

- Paatero, P., Tapper, U., 1994. Positive matrix factorization: A non-negative factor model with optimal utilization of error estimates of data values. *Environmetrics* 5, 111–126. <https://doi.org/10.1002/env.3170050203>
- Pant, P., Harrison, R.M., 2012. Critical review of receptor modelling for particulate matter: A case study of India. *Atmos. Environ.* 49, 1–12. <https://doi.org/10.1016/j.atmosenv.2011.11.060>
- Parekh, P.P., Ghauri, B., Siddiqi, Z.R., Husain, L., 1967. The use of chemical and statistical methods to identify sources of selected elements in ambient air aerosols in Karachi, Pakistan. *Atmos. Environ.* 21, 1267–1274. [https://doi.org/10.1016/0004-6981\(67\)90073-X](https://doi.org/10.1016/0004-6981(67)90073-X)
- POSOCO, 2020. All-India Maximum Demand and Energy Met during Management of COVID -19 in comparison to 2019.
- Rai, P., Furger, M., El Haddad, I., Kumar, V., Wang, L., Singh, A., Dixit, K., Bhattu, D., Petit, J.-E., Ganguly, D., Rastogi, N., Baltensperger, U., Tripathi, S.N., Slowik, J.G., Prévôt, A.S.H., 2020a. Real-time measurement and source apportionment of elements in Delhi’s atmosphere. *Sci. Total Environ.* 140332. <https://doi.org/10.1016/j.scitotenv.2020.140332>
- Rai, P., Furger, M., Slowik, J.G., Canonaco, F., Fröhlich, R., Hüglin, C., Minguillón, M.C., Petterson, K., Baltensperger, U., Prévôt, A.S.H., 2020b. Source apportionment of highly time-resolved elements during a firework episode from a rural freeway site in Switzerland. *Atmos. Chem. Phys.* 20, 1657–1674. <https://doi.org/10.5194/acp-20-1657-2020>
- Reche, C., Viana, M., Amato, F., Alastuey, A., Moreno, T., Hillamo, R., Teinilä, K., Saarnio, K., Seco, R., Peñuelas, J., Mohr, C., Prévôt, A.S.H., Querol, X., 2012. Biomass burning contributions to urban aerosols in a coastal Mediterranean City. *Sci. Total Environ.* 427–428, 175–190. <https://doi.org/10.1016/j.scitotenv.2012.04.012>
- Reddy, M.S., Basha, S., Joshi, H. V., Jha, B., 2005. Evaluation of the emission characteristics of trace metals from coal and fuel oil fired power plants and their fate during combustion. *J. Hazard. Mater.* 123, 242–249. <https://doi.org/10.1016/j.jhazmat.2005.04.008>
- Roy, R., Agarwal, V., 2020. Millions of Indians Are Fleeing Cities, Raising Fears of a Coronavirus ‘Land Mine’ in Villages. *Wall Str. J.*
- Rudnick, L.R., 2017. *Lubricant Additives: Chemistry and Applications*. CRC Press, Taylor & Francis Group.

- Sarkar, S., 2009. *Fuels and Combustion*. CRC Press.
- Seinfeld, J.H. and Pandis, S.N., 2006. *Atmospheric Chemistry and Physics: From Air Pollution to Climate Change*, 2nd ed. John Wiley & Sons, New York.
- Seinfeld, J.H., 2004. Air pollution: A half century of progress. *AIChE J.* 50, 1096–1108.
<https://doi.org/10.1002/aic.10102>
- Selvam, S., Muthukumar, P., Venkatramanan, S., Roy, P.D.D., Manikanda Bharath, K., Jesuraja, K., 2020. SARS-CoV-2 pandemic lockdown: Effects on air quality in the industrialized Gujarat state of India. *Sci. Total Environ.* 737, 140391. <https://doi.org/10.1016/j.scitotenv.2020.140391>
- Sharma, H., Jain, V.K., Khan, Z.H., 2007. Characterization and source identification of polycyclic aromatic hydrocarbons (PAHs) in the urban environment of Delhi. *Chemosphere* 66, 302–310.
<https://doi.org/10.1016/j.chemosphere.2006.05.003>
- Sharma, N., Prakash, R., Srivastava, A., Sadana, U.S., Acharya, R., Prakash, N.T., Reddy, A.V.R., 2009. Profile of selenium in soil and crops in seleniferous area of Punjab, India by neutron activation analysis. *J. Radioanal. Nucl. Chem.* 281, 59–62. <https://doi.org/10.1007/s10967-009-0082-y>
- Sharma, S.K., Mandal, T.K., Jain, S., Saraswati, Sharma, A., Saxena, M., 2016. Source Apportionment of PM_{2.5} in Delhi, India Using PMF Model. *Bull. Environ. Contam. Toxicol.* 97, 286–293. <https://doi.org/10.1007/s00128-016-1836-1>
- Shridhar, V., Khillare, P.S., Agarwal, T., Ray, S., 2010. Metallic species in ambient particulate matter at rural and urban location of Delhi. *J. Hazard. Mater.* 175, 600–607. <https://doi.org/10.1016/j.jhazmat.2009.10.047>
- Sicard, P., De Marco, A., Agathokleous, E., Feng, Z., Xu, X., Paoletti, E., Rodriguez, J.J.D., Calatayud, V., 2020. Amplified ozone pollution in cities during the COVID-19 lockdown. *Sci. Total Environ.* 735.
<https://doi.org/10.1016/j.scitotenv.2020.139542>
- Sohrabi, C., Alsafi, Z., O'Neill, N., Khan, M., Kerwan, A., Al-Jabir, A., Iosifidis, C., Agha, R., 2020. World Health Organization declares global emergency: A review of the 2019 novel coronavirus (COVID-19). *Int. J. Surg.* 76, 71–76. <https://doi.org/10.1016/j.ijisu.2020.02.034>
- Spencer, M.T., Shields, L.G., Sodeman, D.A., Toner, S.M., Prather, K.A., 2006. Comparison of oil and fuel particle chemical signatures with particle emissions from heavy and light duty vehicles. *Atmos. Environ.* 40, 5224–5235.

<https://doi.org/10.1016/j.atmosenv.2006.04.011>

- Srivastava, S., Kumar, A., Baudh, K., Gautam, A.S., Kumar, S., 2020. 21-Day Lockdown in India Dramatically Reduced Air Pollution Indices in Lucknow and New Delhi, India. *Bull. Environ. Contam. Toxicol.*
<https://doi.org/10.1007/s00128-020-02895-w>
- Sun, J., Shen, Z., Zhang, L., Lei, Y., Gong, X., Zhang, Q., Zhang, T., Xu, H., Cui, S., Wang, Q., Cao, J., Tao, J., Zhang, N., Zhang, R., 2019. Chemical source profiles of urban fugitive dust PM_{2.5} samples from 21 cities across China. *Sci. Total Environ.* 649, 1045–1053. <https://doi.org/10.1016/j.scitotenv.2018.08.374>
- Sun, Y., Du, W., Fu, P., Wang, Q., Li, J., Ge, X., Zhang, Q., Zhu, C., Ren, L., Xu, W., Zhao, J., Han, T., Worsnop, D.R., Wang, Z., 2016. Primary and secondary aerosols in Beijing in winter: sources, variations and processes. *Atmos. Chem. Phys.* 16, 8309–8329. <https://doi.org/10.5194/acp-16-8309-2016>
- Sweet, C.W., Vermette, S.J., Landsberger, S., 1993. Sources of toxic trace elements in urban air in Illinois. *Environ. Sci. Technol.* 27, 2502–2510. <https://doi.org/10.1021/es00048a030>
- Thorpe, A., Harrison, R.M., 2008. Sources and properties of non-exhaust particulate matter from road traffic: A review. *Sci. Total Environ.* 400, 270–282. <https://doi.org/10.1016/j.scitotenv.2008.06.007>
- Tobías, A., Carnerero, C., Reche, C., Massagué, J., Via, M., Minguillón, M.C., Alastuey, A., Querol, X., 2020. Changes in air quality during the lockdown in Barcelona (Spain) one month into the SARS-CoV-2 epidemic. *Sci. Total Environ.* 726, 138540. <https://doi.org/10.1016/j.scitotenv.2020.138540>
- Ulbrich, I.M., Canagaratna, M.R., Zhang, Q., Worsnop, D.R., Jimenez, J.L., 2009. Interpretation of organic components from Positive Matrix Factorization of aerosol mass spectrometric data. *Atmos. Chem. Phys.* 9, 2891–2918. <https://doi.org/10.5194/acp-9-2891-2009>
- Vehlow, J., Bergfeldt, B., Hunsinger, H., Scifert, H., Mark, F.E., 2003. Bromine in waste incineration partitioning and influence on metal volatilisation. *Environ. Sci. Pollut. Res.* 10, 329–334.
<https://doi.org/10.1065/espr2003.02.147>
- Volkamer, R., Jimenez, J.L., San Martini, F., Dzepina, K., Zhang, Q., Salcedo, D., Molina, L.T., Worsnop, D.R., Molina, M.J., 2006. Secondary organic aerosol formation from anthropogenic air pollution: Rapid and higher than expected. *Geophys. Res. Lett.* 33, L17811. <https://doi.org/10.1029/2006GL026899>
- Vossler, T., Černíkovský, L., Novák, J., Williams, R., 2016. Source apportionment with uncertainty estimates of fine

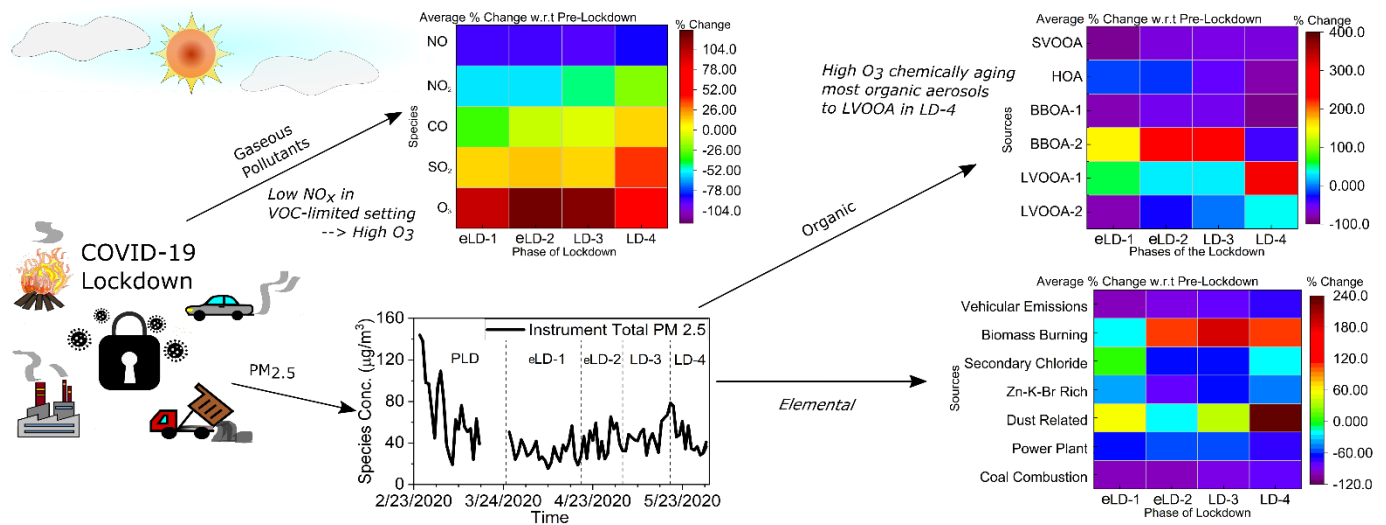
- particulate matter in Ostrava, Czech Republic using Positive Matrix Factorization. *Atmos. Pollut. Res.* 7, 503–512. <https://doi.org/10.1016/j.apr.2015.12.004>
- Warner, J.X., Dickerson, R.R., Wei, Z., Strow, L.L., Wang, Y., Liang, Q., 2017. Increased atmospheric ammonia over the world's major agricultural areas detected from space. *Geophys. Res. Lett.* 44, 2875–2884. <https://doi.org/10.1002/2016GL072305>
- Watson, J.G., Chow, J.C., 2015. Receptor Models and Measurements for Identifying and Quantifying Air Pollution Sources, in: *Introduction to Environmental Forensics*. Elsevier, pp. 677–706. <https://doi.org/10.1016/B978-0-12-404696-2.00020-5>
- Wilson, W.E., Levy, A., Wimmer, D.B., 1972. A Study of Sulfur Dioxide in Photochemical Smog. *J. Air Pollut. Control Assoc.* 22, 27–32. <https://doi.org/10.1080/00022470.1972.10469605>
- Wu, Gamber, Sun, 2020. Does Wuhan Need to be in Lockdown during the Chinese Lunar New Year? *Int. J. Environ. Res. Public Health* 17, 1002. <https://doi.org/10.3390/ijerph17031002>
- Zhang, Q., Rami Alfarra, M., Worsnop, D.R., Allan, J.D., Coe, H., Canagaratna, M.R., Jimenez, J.L., 2005a. Deconvolution and quantification of hydrocarbon-like and oxygenated organic aerosols based on aerosol mass spectrometry. *Environ. Sci. Technol.* 39, 4938–4952. <https://doi.org/10.1021/es048568l>
- Zhang, Q., Worsnop, D.R., Canagaratna, M.R., Jimenez, J.L., 2005b. Hydrocarbon-like and oxygenated organic aerosols in Pittsburgh: insights into sources and processes of organic aerosols. *Atmos. Chem. Phys.* 5, 3289–3311. <https://doi.org/10.5194/acp-5-3289-2005>
- Zhang, T., Cao, J.J., Tie, X.X., Shen, Z.X., Liu, S.X., Ding, H., Han, Y.M., Wang, G.H., Ho, K.F., Qiang, J., Li, W.T., 2011. Water-soluble ions in atmospheric aerosols measured in Xi'an, China: Seasonal variations and sources. *Atmos. Res.* 102, 110–119. <https://doi.org/10.1016/j.atmosres.2011.06.014>
- Zhao, S., Duan, Y., Chen, L., Li, Y., Yao, T., Liu, S., Liu, M., Lu, J., 2017. Study on emission of hazardous trace elements in a 350 MW coal-fired power plant. Part 2. arsenic, chromium, barium, manganese, lead. *Environ. Pollut.* 226, 404–411. <https://doi.org/10.1016/j.envpol.2017.04.009>
- Zheng, H., Kong, S., Chen, N., Yan, Y., Liu, D., Zhu, B., Xu, K., Cao, W., Ding, Q., Lan, B., Zhang, Z., Zheng, M., Fan, Z., Cheng, Y., Zheng, S., Yao, L., Bai, Y., Zhao, T., Qi, S., 2020. Significant changes in the chemical compositions and sources of PM_{2.5} in Wuhan since the city lockdown as COVID-19. *Sci. Total Environ.* 739, 140000. <https://doi.org/10.1016/j.scitotenv.2020.140000>

Zhu, Q., Huang, X.-F., Cao, L.-M., Wei, L.-T., Zhang, B., He, L.-Y., Elser, M., Canonaco, F., Slowik, J.G., Bozzetti, C., El-Haddad, I., Prévôt, A.S.H., 2018. Improved source apportionment of organic aerosols in complex urban air pollution using the multilinear engine (ME-2). *Atmos. Meas. Tech.* 11, 1049–1060.

<https://doi.org/10.5194/amt-11-1049-2018>

Zoller, W.H., Gladney, E.S., Gordon, G.E., Bors, J.J., 1974. Emissions of trace elements from coal fired power plants. *Trace Subst. Environ. Heal.* 8.

Trace Subst. Environ. Heal. 8.



“Graphical Abstract”

Supplementary Information for "Variation in chemical composition and sources of PM_{2.5} during the COVID-19 lockdown in Delhi."

Chirag Manchanda ^a, Mayank Kumar ^{a,*}, Vikram Singh ^{b,*}, Mohd Faisal ^b, Naba Hazarika ^c, Ashutosh Shukla ^d, Vipul Lalchandani ^d, Vikas Goel ^a, Navaneeth Thamban ^d, Dilip Ganguly ^e, Sachchida Nand Tripathi ^{d,*}

a. Department of Mechanical Engineering, Indian Institute of Technology, Delhi, New Delhi, India

b. Department of Chemical Engineering, Indian Institute of Technology, Delhi, New Delhi, India

c. Department of Applied Mechanics, Indian Institute of Technology, Delhi, New Delhi, India

d. Department of Civil Engineering, Indian Institute of Technology, Kanpur, Uttar Pradesh, India

e. Centre for Atmospheric Sciences, Indian Institute of Technology, Delhi, New Delhi, India

S1. Quality Assurance and Quality Control (QA/QC) Procedures

The Xact 625i ambient metals monitor was operated at the standard flow rate of 16.7 lpm while sampling ambient air for PM_{2.5} at an hourly time resolution. The instrument is designed to perform automated quality assurance checks every midnight for the elements Cr, Cd, and Pb. In addition to the automated QA checks, leak and flow checks along with XRF and flow calibration was performed at regular intervals as per the maintenance routine advised by the manufacturer.

The Q-ACSM was operated with a standard flow rate of around 0.1 lpm, while sampling and analyzing NR-PM_{2.5} at a 10-min interval, with background air, allowing for continuous air beam correction, and averaged to an hourly resolution. The collection efficiency (CE) was determined for each spectrum for an optimum collection based on inlet humidity, particle composition, and aerosol acidity, as described by Middlebrook et al. (2012) The ionization efficiency (IE) of NO₃ and relative ionization efficiencies (RIE) of NH₄ and SO₄ were calculated using a monodisperse supply of NH₄NO₃ and (NH₄)₂SO₄ aerosols, selected through a differential mobility analyzer (DMA) and counted using a condensation particle counter (CPC) as suggested by Crenn et al. (2015)

The Aethalometer was run at a standard operating flow rate of 5 lpm, with a 1-minute time resolution, and averaged to an hourly resolution. While the Aethalometer is designed to operate independently with minimal intervention, the routine was performed as per the manufacturer's recommendation. The routine maintenance involved regular flow rate checks, inspection, and cleaning of the optical chamber and insect screen assembly. The measurements were monitored

* Corresponding Authors

E-mail addresses : kmayank@mech.iitd.ac.in (M. Kumar); vs225@chemical@iitd.ac.in (V. Singh), snt@iitk.ac.in (S.N. Tripathi)

continuously for any instrument warnings, noise/spikes, as well as BC vs. attenuation values for any required compensation.

The instruments employed in this study (discussed in section 2.2), are designed to measure partial, rather than total PM_{2.5} as none of the three instruments can measure refractory cations and anions like sodium, magnesium, oxides and fluorides; however, the residual mass is usually noted to be quite low. The measurements from these individual instruments were totaled and regressed against the readings of a collocated BAM measuring total PM_{2.5} for intermittent phases (PLD and LD-3), to check for mass closure. We noted a significant correlation (Pearson R > 0.91) between the total instrument measured particulate mass and the BAM readings, the regression results are presented in figure S1.

S2. Positive Matrix Factorization(PMF) Analysis

S2.1 PMF Input preparation

The elemental species measured using Xact 625i and the organics fraction measured using the Q-ACSM are subjected to PMF-based source apportionment individually. Xact 625i is set to an hourly time resolution, while the Q-ACSM measures and chemically analyzes the particulate matter every 10-minutes, but the measurements are aggregated to hourly resolution for comparison with the Xact 625i measurements.

Some species (elements for Xact or *m/z* ratios for ACSM) were excluded from the PMF input in cases where an appreciable amount of data points (greater than 50%) are below the Minimum Detection Limit (MDL) (Polissar et al., 1998). The MDLs for each measured elemental species were provided by the manufacturer (Cooper Environmental), while the MDL for the organic fragments was determined according to Singla et al. (2017). for Q-ACSM. Missing data points (due to failure in power supply, routine maintenance) were neglected from the PMF input for this study (Rai et al., 2020b).

The quality of measurement of each species *j* was further characterized based on the signal to noise (S/N) ratio calculated within the EPA PMF 5.0 module (Norris et al., 2014). For every concentration value x_{ij} and corresponding uncertainty s_{ij} , the difference between the two is used as the signal d_{ij} , such that :

$$d_{ij} = \left(\frac{x_{ij} - s_{ij}}{s_{ij}} \right) \text{ if } x_{ij} > s_{ij} \dots\dots (1)$$

$$d_{ij} = 0 \text{ if } x_{ij} < s_{ij} \dots\dots (2)$$

(S/N) ratio is then given by Equation 3 as follows:

$$\left(\frac{S}{N}\right)_j = 1/n \sum_1^n d_{ij} \dots \dots (3)$$

The species which had $S/N > 1$ were categorized as strong in data quality. The input concentration and uncertainty were used for further analysis with no modification. The species with S/N between 0.5 and 1 were categorized as weak, and the input uncertainty values were increased by a factor of four and used along with the input concentration for further analysis. Finally, species with an S/N ratio below 0.5 were classified as bad values and were excluded from further analysis.

Xact 625i was set up to quantify 36 elements (Si, S, Cl, K, Ca, Sc, Ti, V, Mn, Fe, Co, Zn, Ga, Ge, As, Se, Br, Rb, Sr, Mo, Pd, Ag, Cd, In, Sn, Sb, Te, Cs, Ba, La, Ce, Au, Hg, Tl, Pb, and Bi) with an hourly time resolution. During the present study 19 elements (Sc, Co, Ga, Ge, Mo, Pd, Ag, Cd, In, Sn, Sb, Te, Cs, La, Ce, Au, Hg, Tl, Bi) were neglected as more than 50% of the data points were below the MDL for the respective species. Xact 625i software reports measurement uncertainty s_{ij} for every measurement, that accounts for the spectral deconvolution uncertainty as well as the sampling uncertainty (Tremper et al., 2018), the same has been employed for the PMF input in this study

The Q-ACSM employed in our study determines quantitative mass spectra of non-refractory (NR) $PM_{2.5}$ (fraction of total $PM_{2.5}$ that flash vaporizes at 600C) up to mass to charge ratios (m/z) of 200 (Crenn et al., 2015; Ng et al., 2011). However, for the present study, the input was restricted to m/z 120, as much lower particle mass was observed for higher m/z 's. The measured spectrum was resolved into nitrate, sulfate, ammonium, and organic fractions using a library of known fragmentation characteristics (Allan et al., 2004). For the ACSM species, the PMF input uncertainty matrix was calculated using the standard Q-ACSM data analysis software following the procedures described in past studies (Ng et al., 2011; Ulbrich et al., 2009).

S2.2 Factor Selection and Uncertainty Quantification

The selection of the number of factors is an essential user-dependent step in any source apportionment study implemented through PMF. However, since the PMF technique is based on minimization of weighted residual error for the linear fitting of a multivariate system of variables (section S1.1), there are often several solutions possible with similar residual structure, leading multiple past studies to conclude that mathematical diagnostics alone were insufficient for choosing the right number of factors (Canonaco et al., 2013; Rai et al., 2020b). Thus, for the present study the in addition to the diagnostics like total Q-value, Q/Q_{exp} (Canonaco et al., 2013) or scaled residuals for each species, we explore the realizability of each resolved factor by comparing the factor time variation with external tracers, known diurnal trends and known elemental contribution or mass spectra reported in previous studies.

For the initial base runs, we examine the solution space, with the number of factors ranging from 3 to 10 with 10 seeds each (number of PMF runs with different pseudorandom starts) for both ACSM and Xact based source apportionment. In the vicinity of the possible optimal solution (lowest Q-value with no significant change with further increment in the number of factors), the process is repeated with 50 seeds each.

The optimal solution in both cases, was tested for rotational ambiguity by subjecting it to DISP analysis available within the EPA PMF 5.0 module. The DISP assess the largest range of solution factor profile values without an appreciable change in the optimal Q-value. In the DISP method, each species in the factor profiles obtained from the base-run are perturbed about the base value, one species at a time and after each adjustment the PMF run is repeated to calculate a new converged solution such that the change in the Q-value, w.r.t the base run remains less than a predetermined maximum change i.e. dQ_{\max} ($dQ_{\max} = 4, 8, 15, 25$). With these changes in the factor profiles, it is possible that the modified factor profile may switch identity when compared to the base run factors i.e. a particular factor from the base run after displacement of certain species may be better correlated to some other base factor than itself, such a case is noted as a factor swap. The EPA PMF module accounts for factor swaps using uncentered cross correlations between the displaced solution and the base run. In the present study no factor swaps were reported for both the Xact-based and ACSM-based PMF solutions. The largest decrease in Q-value for the Xact-based PMF was found to be 0.0668 with % dQ change as 0.002%. For the ACSM-based source apportionment the largest decrease in Q-value was observed to be 0.2028 with % dQ change as 0.0032%. As per Norris et al. (2014) % dQ change under 1% represents an acceptable DISP solution, representing reliable PMF solution.

However, the optimal base run solutions was further subjected to variation in f-peak values from -1 to +1 at an increment of 0.1 to explore the rotations of plausible solutions, to evaluate the effect of rotations on the fraction of variance explained by each factor, correlation of factors' mass spectra (MS) with reference mass spectra (for ACSM), correlation of factor time series with external tracers and the mutual correlation between the time series of resolved factors (Bhandari et al., 2020; Rai et al., 2020b; Ulbrich et al., 2009). The range of f-peak rotations was limited to ensure that the rotated solution remains in the vicinity (similar total Q-value) of the initial solution (except the case of a rotationally ambiguous solution) in the solution space.

For the Xact-based source apportionment, no appreciable change in the factor source profiles, and external correlation was observed by varying f-peak; thus, the base solution was chosen as optimal. However, for the ACSM-based source, apportionment rotations were found to improve correlations between factor MS of all factors and reference MS from Ng et al. (2011) and also decrease mutual correlations between the resolved factors. Thus the rotated solution with the

best correlations with reference MS and minimal mutual correlations among factors was chosen to be optimal (Bhandari et al., 2020; Rai et al., 2020b).

Further, the effect of random errors were evaluated using the bootstrap (BS) randomized resampling strategy (Brown et al., 2015; Efron, 1979). The bootstrap is implemented using US EPA PMF 5.0 by a random selection of non-overlapping blocks of species measurements from the input data set and creates a new PMF input matrix with the total number of samples equal to the original input matrix, where the user specifies the block size. The PMF code then runs over the new input matrix, and the BS factors are then mapped to the primary factors. The BS factors are assigned to corresponding base factors with which have the highest uncentered correlation values (above a user-specified threshold). If a particular BS factor doesn't have an uncentered-correlation higher than the threshold with any base factor, then it is considered to be "unmapped." This analysis provides us with a proxy to understand the uncertainty associated with the solution and the apportionment of each species in the resolved factors.

In the present study, the optimal solutions were subjected to 800 BS runs each, with a threshold correlation of 0.8, and more than 764 BS runs were classified as good solutions, having no unmapped factors.

S3. Supplementary Results

The COVID-induced lockdown in India, lasted over a period of 70 days starting 25th March 2020 up to 31st May 2020. The lockdown progressed in a phased manner, during the first phase of the lockdown (LD-1) starting 25th March until 14th April marked the strictest phase of the lockdown, with nearly all services and commercial activities completely suspended, with an exception to providers of essential goods and services like hospitals, grocery stores, and pharmacies. The lockdown was extended with phase-2 (LD-2) lasting up to 3rd April 2020. However, the first set of relaxations were implemented starting 20th April 2020 with allowances to agricultural industries, farming supplies, cargo services. In order to capture the impact of these relaxations in the present study, we focus on eLD-1 and eLD-2, as defined in section 2.1, instead of LD-1 and LD-2. With the start of LD-3 from 4th May 2020, most regions were subdivided into green, orange, and red-zones based on the intensity of the spread of the virus in the region. In green zones, normal movement was restored with public buses running at 50% capacity, only movement with private vehicles was allowed in orange zones, and no relaxations in red zones. LD-4 started on 18th May with further increase in relaxations, the interstate movement was permitted, all categories of small-scale shops were allowed to open, and all industries allowed to restart, private offices were allowed to reopen with 33% staff.

The following sections draw further support to the main manuscript, evaluating the impact of the aforementioned phased relaxations in the lockdown on the variation of sources contributing to ambient PM_{2.5}:

S3.1 Time variation of different aerosols during lockdown

S3.1.1 $PM_{2.5}$ and its constituents

Analyzing the daily average time variation of the instrument total $PM_{2.5}$ and the fractional contribution of each constituent (Figure 1(a)), as discussed earlier in section 3, we note that the average $PM_{2.5}$ values fall by 53.6% from pre-lockdown to lockdown phase-1. We can also observe that each of the $PM_{2.5}$ constituents, i.e., elements, sulfate, nitrate and ammonium (SNA), black carbon (BC), and organics, is found to decrease by 31%, 67.7%, 77.2%, and 47.8% respectively, between PLD and lockdown eLD-1 (Figure 1(b)). However, chloride remains almost unaffected or minimally affected, with only a 12% decrease due to the lockdown.

From Figure 1 (a) and Figure 1 (b), we can also note that total $PM_{2.5}$ along with the elements, SNA, BC, and organics steadily trend back towards their initial concentrations with increasing relaxations in subsequent phases of the lockdown. However, even in the final phase of the lockdown, total $PM_{2.5}$ was 33% lower when compared to the PLD values, while SNA, BC, and organics remained 59.8%, 59.5%, and 19.2% lower than their PLD concentrations.

While average chloride concentration was 46% lower in LD-4 as compared to the pre-lockdown phase, it seems to be affected more by metrological conditions rather than the lockdown. Firstly, chloride concentration was only marginally affected in eLD-1; also, it reached its minimum average concentration ($1.8 \mu\text{g}/\text{m}^3$) in eLD-2 rather than eLD-1 (Figure 1 (b)). This coincides with the observation that a significant portion of eLD-2 and beginning of LD-3 is affected by disturbances from the southeast (from the wind direction/wind speed, Figure S2(a)). This dependence of chloride on wind direction or other metrological conditions is concomitant with the observations made for the apportioned secondary chloride factor in section 3.1.3. Also, it is interesting to note that the elemental concentration increased by 65% in LD-4 w.r.t the PLD concentrations. This could possibly be due to the increase in gust/dust storm events during LD-4 leading to the rise in apportioned dust factor, as discussed in section 3.1.5.

S3.1.2 Gaseous pollutants

In Figure 1 (c) & (d) we plot the concentrations of gaseous pollutants (SO_2 , NO_2 , NO , and CO) taken from the Continuous Ambient Air Quality Monitoring Station (CAAQMS) at RK Puram. As discussed in section 3 and presented in Figure S6(a), a significant drop in NO_2 and NO concentrations 56% and 90%, respectively, after the lockdown, while NO_2 seems to rise back with increasing relaxations, NO concentrations do not rise at the same pace. During LD-4, the average NO_2 levels were 22% lower than its pre-lockdown concentration, while for NO , the average concentration was 85% lower than its PLD average. Transportation is believed to be the primary source of both NO and NO_2 emissions in

Delhi (Tyagi et al., 2016). Similar anomalies have been reported by Nagpure et al. (2013) and Badarinath et al. (2009) in Delhi. However, the disparate behavior could stem from chain reactions initiated by the attack of hydroxyl radical on VOCs and CO catalyzing the conversion of NO to NO₂ (Tiwari et al., 2015), outside the photo stationary state of reactions between NO, NO₂, and O₃ as described by Leighton (1961).

Similarly, CO also follows the intuitive trend of a sudden reduction (by 32%) in LD-4, followed by a gradual increase with increasing relaxations in the lockdown. It is again interesting to note that SO₂ remains mostly unaffected by the lockdown based on measurements for the RK Puram station; this is in line with a recent study by Kumari and Toshniwal (2020), where only a slight decrease in SO₂ was reported for Delhi, Kumari and co-workers supported this observation with the hypothesis that SO₂ in Delhi mainly stems from power plant emissions which have remained unaffected by the lockdown. The negligible effect of transportation on SO₂ is also supported by the fact that BS VI fuel with low sulfur content is already in use in Delhi since 2019 (Confederation of Indian Industries (CII) and NITI Aayog, 2018).

In Figure S2(b), we further analyze the effect of the lockdown on ambient air quality based on aerosol neutralization ratio (ANR), as defined by Zhang et al. (2007). The ANR was found to be weakly affected by the lockdown for the PLD phase; the average ANR was 0.83, followed by 0.73, 0.77, 0.78, 0.78 for each of eLD-1 to LD-4. The ANR indicated weak acidity associated with the aerosols, which is slightly intensified by the lockdown, followed by a gradual trend back towards the PLD value.

S3.1.3 Markers for organic sources

While section 3.2 elaborates on the source apportionment of the organic fraction of the particulate matter, in Figure S2(b), we plot some significant m/z ratios as tracers to known apportioned factors like m/z 43 for semi-volatile OOA (SVOOA) and m/z 44 for low volatility OOA (LVOOA), m/z 60 & m/z 73 for Biomass Burning Organic Aerosol (BBOA) and m/z 55 & m/z 57 for Hydrocarbon like Organic Aerosol (HOA). Interestingly, we observe that most of these m/z 's decrease significantly during lockdown phase-4, while m/z 44 increases significantly for the same period. Usually, m/z 55 and m/z 57 and the apportioned factor marked by them, i.e., HOA, is found to correlate well with vehicular markers like BC (DeWitt et al., 2015), however, in the present case, the reduction in gaseous pollutants like NO₂ and NO, also associated with vehicular origin (Tyagi et al., 2016), due to the lockdown is much more intense than observed in m/z 55 or 57, supporting possible alternate sources for the same during the lockdown as discussed in section 3.2 with the source apportionment of the organic PM_{2.5}.

S3.2 Diurnal Variation of Factors apportioned using PMF

The details on the factors resolved from source apportionment of Xact and ACSM derived species are discussed in section 3.1 and 3.2, respectively. In this section, we present the diurnality associated with each resolved factor and the implications associated with the same.

Figure S4 displays the diurnal variation of each factor constituting elemental PM_{2.5}, for each phase from PLD to LD-4. The vehicular emissions factor shows appreciable diurnal variation during PLD and LD-4, with significant peaks around 6:00 IST to 8:00 IST and also a relatively weaker peak around 18:00 IST to 21:00 IST, both of which correspond to traffic rush hours in the vicinity of the sampling location; also some peaks after midnight may signal toward the heavy-duty vehicular movement (for logistics and transportation) during the night. However, it is essential to note that the lockdown severely impacts this typical diurnality associated with this factor, and no characteristic peaks are observed during eLD-1 to LD-4, it is essential to consider that the average factor concentration was noted to drop by 96% as discussed in section 3.1. Also, the restricted vehicular movement during the lockdown is not expected to follow a significant trend, justifying the atypical nature of the diurnal pattern.

The biomass burning factor is found to peak in the early morning around 6:00 IST, indicating the influence of gas-particle partitioning and ambient temperature on the time variation of this factor, which is in line with the findings of past studies (Rai et al., 2020a). Also, the nature of the diurnal profile has remained very similar during all phases of the lockdown, indicating a less pronounced effect of the lockdown on the nature of the source.

The diurnality associated with the secondary chloride factor is discussed in section 3.1.3 and is indicative of dependence of the concentration on gas-particle due to increment in volatility and consequent evaporation after sunrise supporting the significant peak around 6:00 IST followed by the rapid decline in concentration. The Zn-K- Br rich factor is found to have diurnal behavior similar to secondary chloride and could partially contribute to the same as a potential source of HCl and HBr, as discussed in section 3.1.3 and 3.1.4. However, it is vital to take into account that secondary chloride remained mostly unaffected by the lockdown, while the Zn-K-Br rich source was found to drop by 42% in eLD-1.

In the present study, while the lockdown is found to have little or no impact on the dust-related factor in terms of the concentration, however, there is significant variation in the diurnal pattern of the same across different phases of the lockdown. But since this factor is expected to be influenced by a variety of metrological and transport problems, it is difficult to attribute the variation to a single cause.

The power plants factor is found to have a relatively weak diurnal variation; the S-rich factor was noted to correlate well with SOR in section 3.1.5, indicating the factor to be driven by sulfate emissions, the weak diurnality can be attributed

to the low volatility associated with sulfate; also the peaks around 8:00 IST indicate the rise in factor concentration due to photo-oxidation from SO_2 to SO_4^{2-} , along with gas-particle partitioning of compounds like $(\text{NH}_4)_2\text{SO}_4$.

The coal combustion diurnal profile displays a peak around 6:00 IST, similar to secondary chloride signaling towards the role of gas-particle partitioning in giving rise to the observed diurnality.

The diurnal variation profiles of the factors resolved from the source apportionments of organic fraction of NR-PM_{2.5} are collated in Figure S5. The diurnal variation of SVOOA has been discussed in section 3.2.1 and is found to be dependent on photo-oxidation and boundary layer height. The diurnal profile of HOA is typical of a primary organic aerosol with seeming high dependence on boundary layer height, leading to a rise in concentration when the boundary layer height is lower, i.e., during the night and following a decrease in the morning when the boundary layer rises. Overall the diurnal profile has no discernable rush hour peaks to attribute the factor to have a vehicular origin.

Similar to HOA, both BBOA-1 and BBOA-2 display diurnal behavior characteristic of primary organic emissions and their dependence on boundary layer height or ambient temperature (Bhandari et al., 2020), however BBOA-2 in addition to the increased concentration during the night, also presents a distinct peak around 6:00 IST - 9:00 IST, similar to biomass burning factor from Xact source apportionment, indicating the role of gas-particle partitioning or a primary emission associated with that time.

LVOOA-2 shows a weak diurnal behavior which is characteristic of LVOOA as noted by previous studies (Aiken et al., 2009; Zhu et al., 2018), and is attributed to the low-volatility associated with this factor; the factor observes a small peak around noon due to enhanced photo-oxidation/ photochemical aging of other organic aerosols, in turn, is converted into LVOOA. However, as discussed in section 3.2.4, LVOOA-1 display diurnal behavior similar to primary organic aerosols, and this behavior is further intensified during LD-4 when the highest average concentration corresponding to this factor is recorded. This anomalous behavior indicates the local formation/emission of LVOOA rather than the typical aging route citing the atypical diurnal as well as other factors discussed in section 3.2.4

References

Aiken, A.C., Salcedo, D., Cubison, M.J., Huffman, J.A., DeCarlo, P.F., Ulbrich, I.M., Docherty, K.S., Sueper, D., Kimmel, J.R., Worsnop, D.R., Trimborn, A., Northway, M., Stone, E.A., Schauer, J.J., Volkamer, R.M., Fortner, E., de Foy, B., Wang, J., Laskin, A., Shutthanandan, V., Zheng, J., Zhang, R., Gaffney, J., Marley, N.A., Paredes-Miranda, G., Arnott, W.P., Molina, L.T., Sosa, G., Jimenez, J.L., 2009. Mexico City aerosol analysis during MILAGRO using high resolution aerosol mass spectrometry at the urban supersite (T0) – Part 1: Fine

particle composition and organic source apportionment. *Atmos. Chem. Phys.* 9, 6633–6653.

<https://doi.org/10.5194/acp-9-6633-2009>

Allan, J.D., Delia, A.E., Coe, H., Bower, K.N., Alfarra, M.R., Jimenez, J.L., Middlebrook, A.M., Drewnick, F., Onasch, T.B., Canagaratna, M.R., Jayne, J.T., Worsnop, D.R., 2004. A generalised method for the extraction of chemically resolved mass spectra from Aerodyne aerosol mass spectrometer data. *J. Aerosol Sci.* 35, 909–922.

<https://doi.org/10.1016/j.jaerosci.2004.02.007>

Badarinath, K.V.S., Sharma, A.R., Kharol, S.K., Prasad, V.K., 2009. Variations in CO, O₃ and black carbon aerosol mass concentrations associated with planetary boundary layer (PBL) over tropical urban environment in India. *J. Atmos. Chem.* 62, 73–86. <https://doi.org/10.1007/s10874-009-9137-2>

Bhandari, S., Gani, S., Patel, K., Wang, D.S., Soni, P., Arub, Z., Habib, G., Apte, J.S., Hildebrandt Ruiz, L., 2020.

Sources and atmospheric dynamics of organic aerosol in New Delhi, India: insights from receptor modeling.

Atmos. Chem. Phys. 20, 735–752. <https://doi.org/10.5194/acp-20-735-2020>

Brown, S.G., Eberly, S., Paatero, P., Norris, G.A., 2015. Methods for estimating uncertainty in PMF solutions: Examples with ambient air and water quality data and guidance on reporting PMF results. *Sci. Total Environ.* 518–519, 626–635. <https://doi.org/10.1016/j.scitotenv.2015.01.022>

Canonaco, F., Crippa, M., Slowik, J.G., Baltensperger, U., Prévôt, A.S.H., 2013. SoFi, an IGOR-based interface for the efficient use of the generalized multilinear engine (ME-2) for the source apportionment: ME-2 application to aerosol mass spectrometer data. *Atmos. Meas. Tech.* 6, 3649–3661. <https://doi.org/10.5194/amt-6-3649-2013>

Confederation of Indian Industries (CII) and NITI Aayog, 2018. Action Plan for Clean Fuel.

Crenn, V., Sciare, J., Croteau, P.L., Verlhac, S., Fröhlich, R., Belis, C.A., Aas, W., Äijälä, M., Alastuey, A., Artiñano, B., Baisnée, D., Bonnaire, N., Bressi, M., Canagaratna, M., Canonaco, F., Carbone, C., Cavalli, F., Coz, E., Cubison, M.J., Esser-Gietl, J.K., Green, D.C., Gros, V., Heikkinen, L., Herrmann, H., Lunder, C., Minguillón, M.C., Močnik, G., O'Dowd, C.D., Ovadnevaite, J., Petit, J.-E., Petralia, E., Poulain, L., Priestman, M., Riffault, V., Ripoll, A., Sarda-Estève, R., Slowik, J.G., Setyan, A., Wiedensohler, A., Baltensperger, U., Prévôt, A.S.H., Jayne, J.T., Favez, O., 2015. ACTRIS ACSM intercomparison – Part 1: Reproducibility of concentration and fragment results from 13 individual Quadrupole Aerosol Chemical Speciation Monitors (Q-ACSM) and consistency with co-located instruments. *Atmos. Meas. Tech.* 8, 5063–5087. <https://doi.org/10.5194/amt-8-5063-2015>

- DeWitt, H.L., Hellebust, S., Temime-Roussel, B., Ravier, S., Polo, L., Jacob, V., Buisson, C., Charron, A., André, M., Pasquier, A., Besombes, J.L., Jaffrezo, J.L., Wortham, H., Marchand, N., 2015. Near-highway aerosol and gas-phase measurements in a high-diesel environment. *Atmos. Chem. Phys.* 15, 4373–4387.
<https://doi.org/10.5194/acp-15-4373-2015>
- Efron, B., 1979. Bootstrap Methods: Another Look at the Jackknife. *Ann. Stat.* 7, 1–26.
<https://doi.org/10.1214/aos/1176344552>
- Kumari, P., Toshniwal, D., 2020. Impact of lockdown measures during COVID-19 on air quality– A case study of India. *Int. J. Environ. Health Res.* 00, 1–8. <https://doi.org/10.1080/09603123.2020.1778646>
- Leighton, P., 1961. *Photochemistry of Air Pollution*.
- Middlebrook, A.M., Bahreini, R., Jimenez, J.L., Canagaratna, M.R., 2012. Evaluation of Composition-Dependent Collection Efficiencies for the Aerodyne Aerosol Mass Spectrometer using Field Data. *Aerosol Sci. Technol.* 46, 258–271. <https://doi.org/10.1080/02786826.2011.620041>
- Nagpure, A.S., Sharma, K., Gurjar, B.R., 2013. Traffic induced emission estimates and trends (2000–2005) in megacity Delhi. *Urban Clim.* 4, 61–73. <https://doi.org/10.1016/j.uclim.2013.04.005>
- Ng, N.L., Herndon, S.C., Trimborn, A., Canagaratna, M.R., Croteau, P.L., Onasch, T.B., Sueper, D., Worsnop, D.R., Zhang, Q., Sun, Y.L., Jayne, J.T., 2011. An Aerosol Chemical Speciation Monitor (ACSM) for Routine Monitoring of the Composition and Mass Concentrations of Ambient Aerosol. *Aerosol Sci. Technol.* 45, 780–794. <https://doi.org/10.1080/02786826.2011.560211>
- Norris, G., Duvall, R., Brown, S., Bai, S., 2014. EPA PMF 5.0 User Guide.
- Polissar, A. V., Hopke, P.K., Paatero, P., Malm, W.C., Sisler, J.F., 1998. Atmospheric aerosol over Alaska: 2. Elemental composition and sources. *J. Geophys. Res. Atmos.* 103, 19045–19057.
<https://doi.org/10.1029/98JD01212>
- Rai, P., Furger, M., El Haddad, I., Kumar, V., Wang, L., Singh, A., Dixit, K., Bhattu, D., Petit, J.-E., Ganguly, D., Rastogi, N., Baltensperger, U., Tripathi, S.N., Slowik, J.G., Prévôt, A.S.H., 2020a. Real-time measurement and source apportionment of elements in Delhi’s atmosphere. *Sci. Total Environ.* 140332.
<https://doi.org/10.1016/j.scitotenv.2020.140332>
- Rai, P., Furger, M., Slowik, J.G., Canonaco, F., Fröhlich, R., Hüglin, C., Minguillón, M.C., Petterson, K.,

- Baltensperger, U., Prévôt, A.S.H., 2020b. Source apportionment of highly time-resolved elements during a firework episode from a rural freeway site in Switzerland. *Atmos. Chem. Phys.* 20, 1657–1674.
<https://doi.org/10.5194/acp-20-1657-2020>
- Singla, V., Mukherjee, S., Safai, P.D., Meena, G.S., Dani, K.K., Pandithurai, G., 2017. Role of organic aerosols in CCN activation and closure over a rural background site in Western Ghats, India. *Atmos. Environ.* 158, 148–159. <https://doi.org/10.1016/j.atmosenv.2017.03.037>
- Tiwari, S., Dahiya, A., Kumar, N., 2015. Investigation into relationships among NO, NO₂, NO_x, O₃, and CO at an urban background site in Delhi, India. *Atmos. Res.* 157, 119–126. <https://doi.org/10.1016/j.atmosres.2015.01.008>
- Tremper, A.H., Font, A., Priestman, M., Hamad, S.H., Chung, T.-C., Pribadi, A., Brown, R.J.C., Goddard, S.L., Grassineau, N., Petterson, K., Kelly, F.J., Green, D.C., 2018. Field and laboratory evaluation of a high time resolution x-ray fluorescence instrument for determining the elemental composition of ambient aerosols. *Atmos. Meas. Tech.* 11, 3541–3557. <https://doi.org/10.5194/amt-11-3541-2018>
- Tyagi, S., Tiwari, S., Mishra, A., Hopke, P.K., Attri, S.D., Srivastava, A.K., Bisht, D.S., 2016. Spatial variability of concentrations of gaseous pollutants across the National Capital Region of Delhi, India. *Atmos. Pollut. Res.* 7, 808–816. <https://doi.org/10.1016/j.apr.2016.04.008>
- Ulbrich, I.M., Canagaratna, M.R., Zhang, Q., Worsnop, D.R., Jimenez, J.L., 2009. Interpretation of organic components from Positive Matrix Factorization of aerosol mass spectrometric data. *Atmos. Chem. Phys.* 9, 2891–2918. <https://doi.org/10.5194/acp-9-2891-2009>
- Zhang, Q., Jimenez, J.L., Worsnop, D.R., Canagaratna, M., 2007. A Case Study of Urban Particle Acidity and Its Influence on Secondary Organic Aerosol. *Environ. Sci. Technol.* 41, 3213–3219.
<https://doi.org/10.1021/es061812j>
- Zhu, Q., Huang, X.-F., Cao, L.-M., Wei, L.-T., Zhang, B., He, L.-Y., Elser, M., Canonaco, F., Slowik, J.G., Bozzetti, C., El-Haddad, I., Prévôt, A.S.H., 2018. Improved source apportionment of organic aerosols in complex urban air pollution using the multilinear engine (ME-2). *Atmos. Meas. Tech.* 11, 1049–1060.
<https://doi.org/10.5194/amt-11-1049-2018>

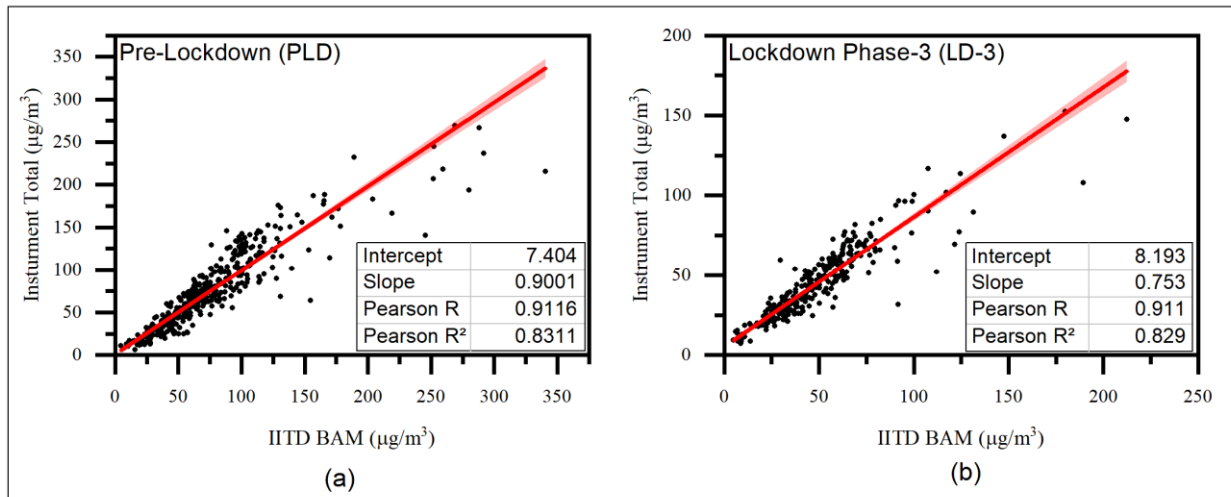


Figure S1: Linear regression analysis between sum of total PM_{2.5} as measured by Xact, ACSM and Aethalometer and a co-located Beta Attenuation Monitor (BAM)

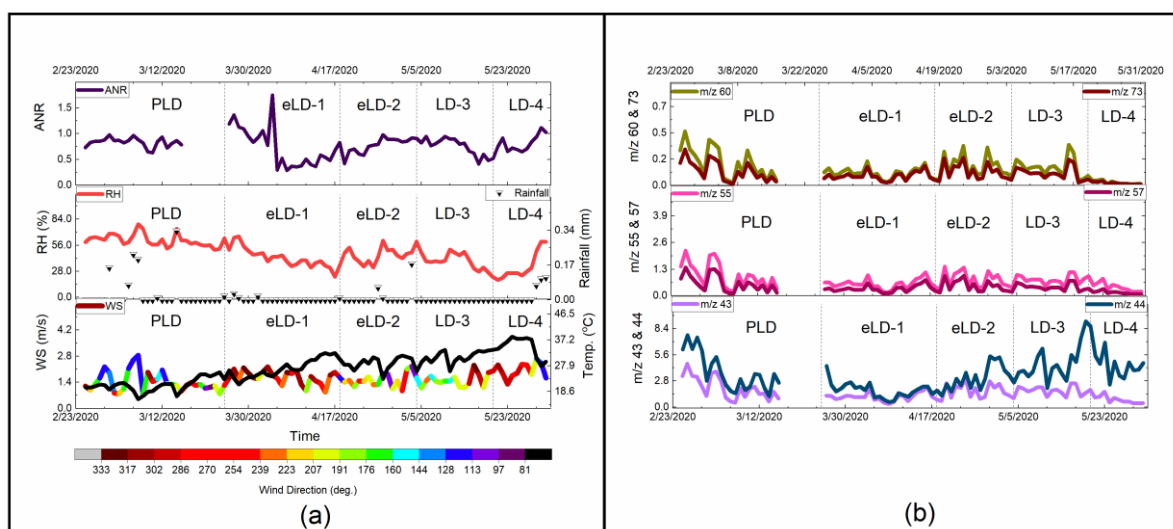


Figure S2: (a) Time variation of ANR, RH WS, WD and ambient temperature through different phases of the lockdown; (b) Time variation of characteristic m/z ratios i.e. 60, 73, 55, 57, 43 and 44 amu, through different phases of the lockdown

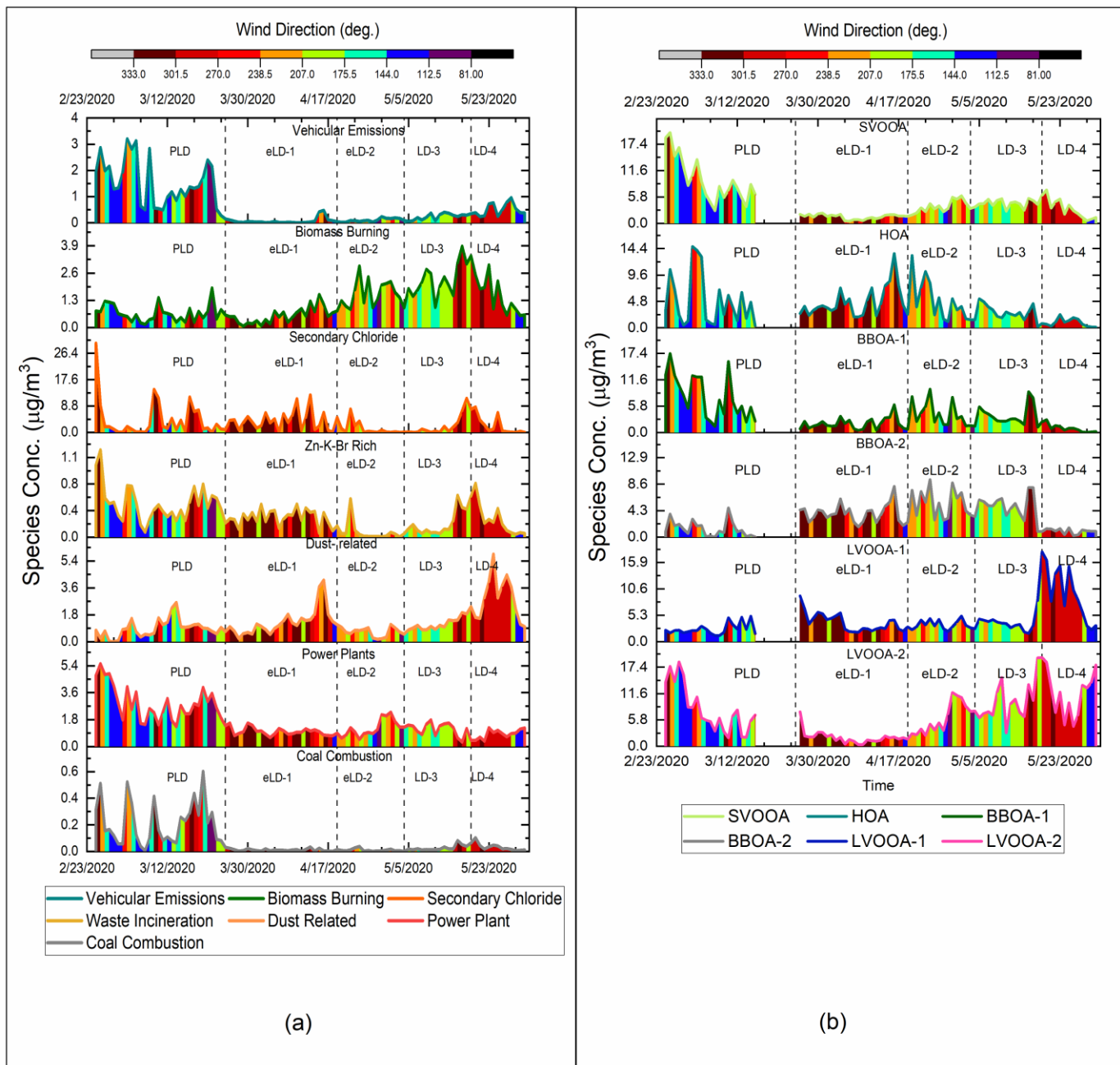


Figure S3: (a) Temporal variation of sources contributing to elemental $\text{PM}_{2.5}$ through different lockdown phases (b) Temporal variation of sources contributing to organic $\text{PM}_{2.5}$ during different lockdown phases

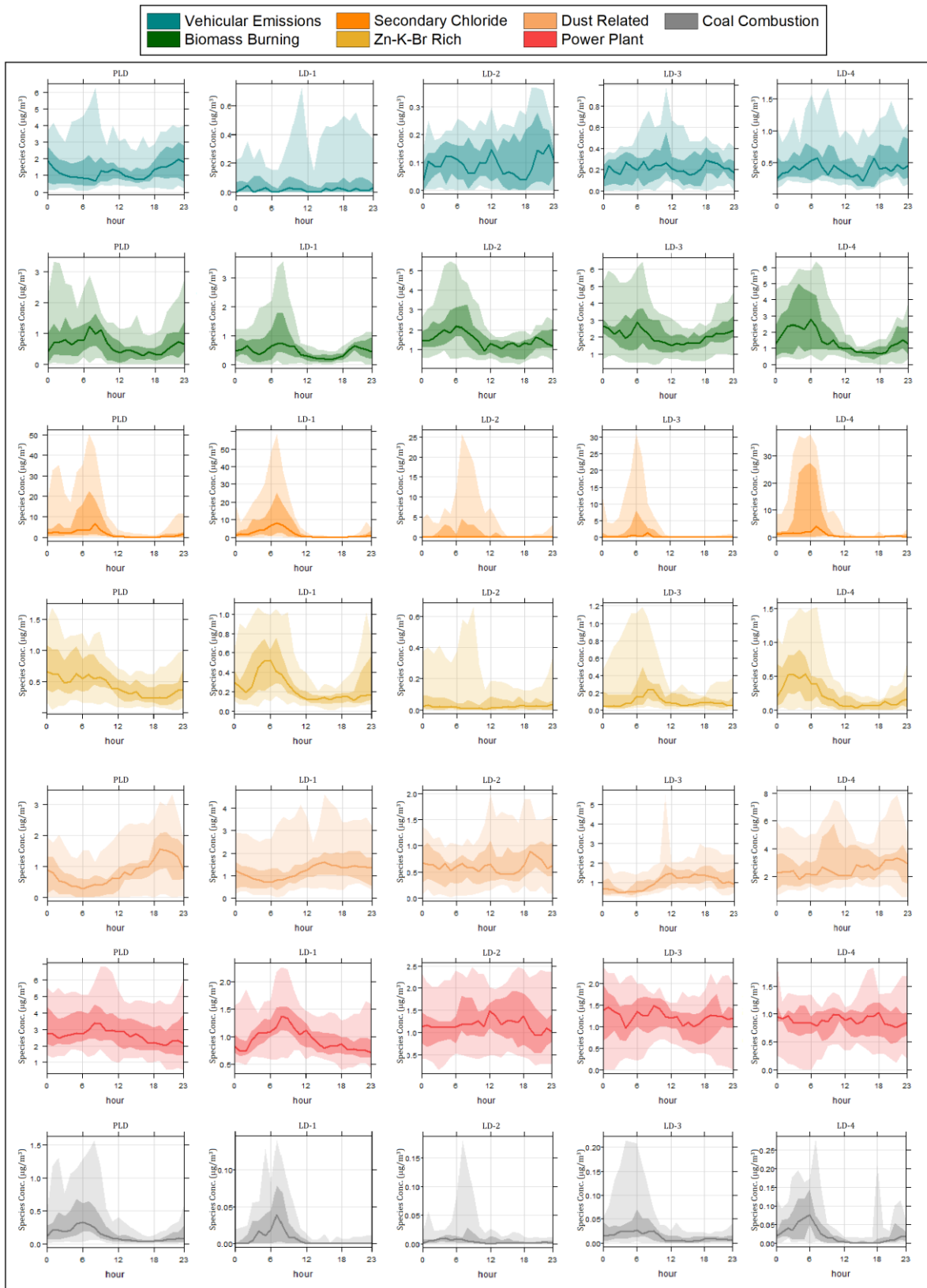


Figure S4: Diurnal Variation of factors resolved from source apportionment of elemental PM_{2.5} (median, 25/75th & 5/95th quantiles)

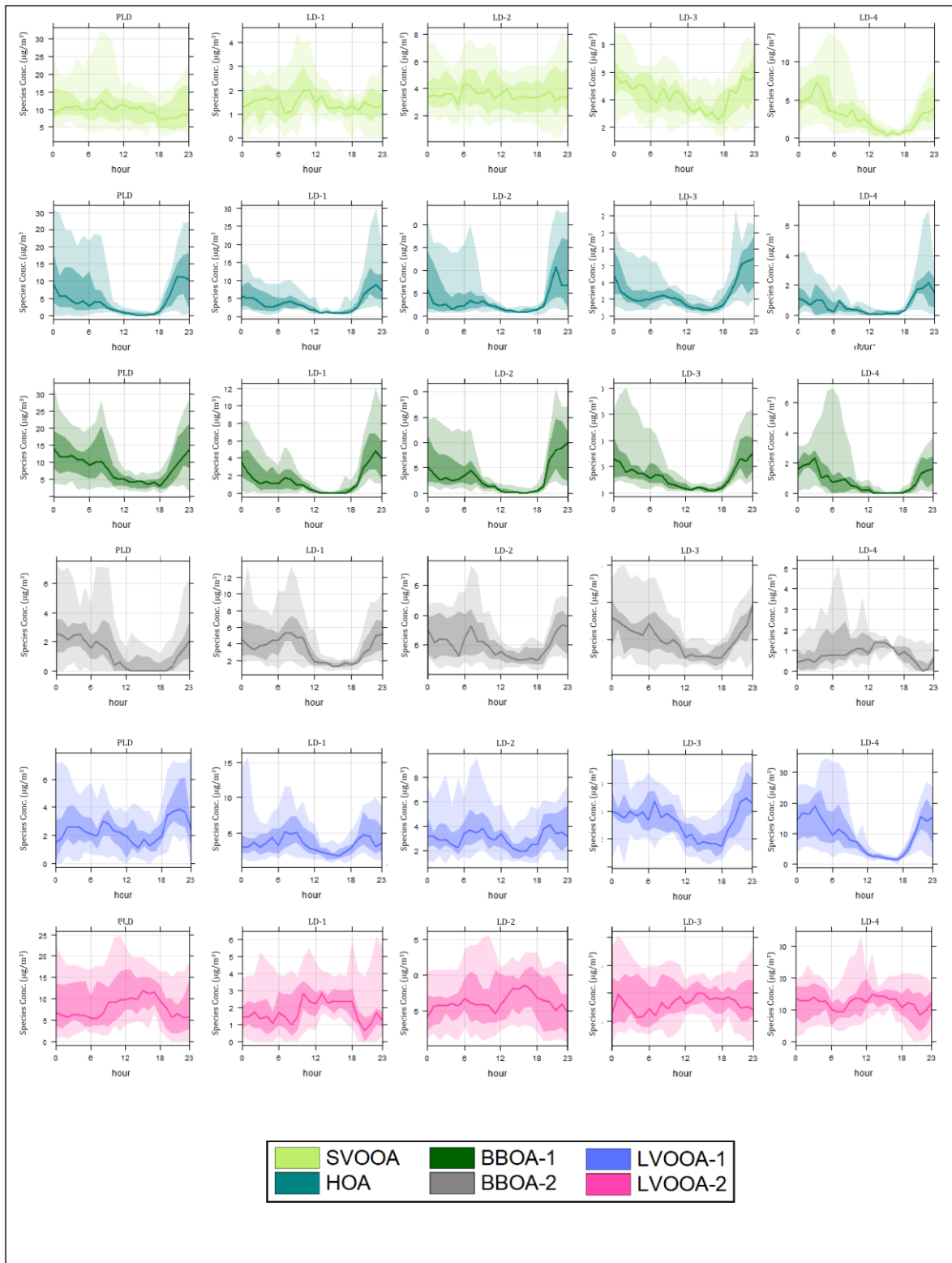


Figure S5: Diurnal Variation of factors resolved from source apportionment of organic NR-PM_{2.5} (median, 25/75th & 5/95th quantiles)

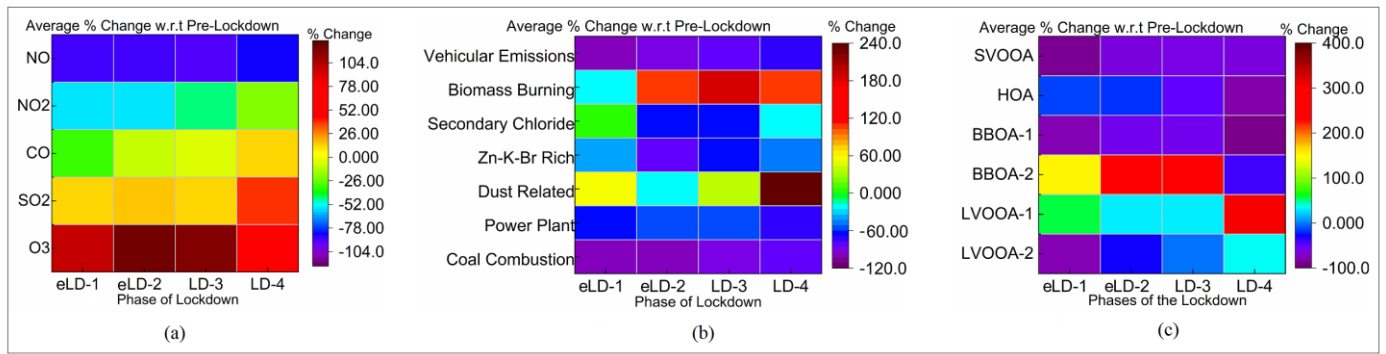


Figure S6: (a) % Change in average gaseous concentrations through each phase of the lockdown w.r.t. pre-lockdown levels; (b) % Change in average concentration of sources contributing to elemental PM_{2.5} through each phase of the lockdown w.r.t. pre-lockdown levels; (c) % Change in average concentration of sources contributing to organic PM_{2.5} through each phase of the lockdown w.r.t. pre-lockdown levels